Rethinking How External Pressure Can Suppress Dendrites in Lithium Metal Batteries

Xin Zhang,[1] Q. Jane Wang,[1,z] Katharine L. Harrison,[2] Katherine Jungjohann,[3] Brad L. Boyce,[3] Scott A. Roberts,[4,*] Peter M. Attia,[5,] and Stephen J. Harris[6,z]**

[1]*Mechanical Engineering Department, Northwestern University, Evanston, Illinois 60208, USA*
[2]*Nanoscale Sciences, Sandia National Laboratories, Albuquerque, New Mexico 87123, USA*
[3]*Center for Integrated Nanotechnologies, Sandia National Laboratories, Albuquerque, New Mexico 87123, USA*
[4]*Engineering Sciences Center, Sandia National Laboratories, Albuquerque, New Mexico 87123, USA*
[5]*Department of Materials Science and Engineering, Stanford University, Stanford, California 94305, USA*
[6]*Materials Science Division, Lawrence Berkeley National Laboratory, Berkeley, California 94720, USA*

We offer an explanation for how dendrite growth can be inhibited when Li metal pouch cells are subjected to external loads, even for cells using soft, thin separators. We develop a contact mechanics model for tracking Li surface and sub-surface stresses where electrodes have realistically (micron-scale) rough surfaces. Existing models examine a single, micron-scale Li metal protrusion under a fixed local current density that presses more or less conformally against a separator or stiff electrolyte. At the larger, sub-mm scales studied here, contact between the Li metal and the separator is heterogeneous and far from conformal for surfaces with realistic roughness: the load is carried at just the tallest asperities, where stresses reach tens of MPa, while most of the Li surface feels no force at all. Yet, dendrite growth is suppressed over the entire Li surface. To explain this dendrite suppression, our electrochemical/mechanics model suggests that Li avoids plating at the tips of growing Li dendrites if there is sufficient local stress; that local contact stresses there may be high enough to close separator pores so that incremental Li^+ ions plate elsewhere; and that creep ensures that Li protrusions are gradually flattened. These mechanisms cannot be captured by single-dendrite-scale analyses.
 [DOI: 10.1149/2.0701914jes]

Manuscript submitted June 25, 2019; revised manuscript received August 21, 2019. Published November 4, 2019.

Using lithium (Li) metal anodes is a focus of next-generation batteries due to their high capacity.[1–3] However, the development of Li-metal batteries with liquid electrolytes, the focus of this work, has encountered a number of problems,[4–6] such as loss of active Li (loss of capacity) as the Li reacts with the electrolyte; and formation and growth of Li protrusions (commonly referred to as dendrites), which results in "dead" Li. Li protrusions can also penetrate through the separator and cause a short circuit,[2,7–11] potentially resulting in a fire.[12]

A number of experimental observations[3,5,13–15] have shown that applying an external mechanical force on a Li metal pouch cell with a liquid electrolyte can inhibit dendrite growth, thereby reducing capacity loss, extending life, and improving safety. To understand this behavior, analytical and numerical studies have been undertaken to describe the influence of local mechanical stresses on dendrite initiation and growth, including phase field models,[16,17] which study dynamics at the interfaces between the electrolyte and dendrites; surface-tension models,[18–21] which study the conditions for dendrite initiation and growth velocity in liquid electrolytes; Brownian statistical models,[22–25] which analyze the morphology evolution of deposited species; and the Chazalviel electromigration-limited model,[9,26–28] which considers that dendrite initiation is induced by an electrodeposition process.

The most widely used model for understanding how mechanical forces inhibit dendrite growth is that proposed by Monroe and Newman.[19,29] This model assumes that a growing Li protrusion (incipient dendrite) under a fixed current density pushes against a polymer electrolyte or separator such that they are in perfect or near-perfect (conformal) contact, and it calculates minimum mechnical properties of the polymer such that Li protrusions do not grow in length. Srinivasan et al.[30] have recently proposed extensions of this model by relaxing many of the assumptions in the Monroe-Newman model and applied them to soft gel, polymer, and ceramic electrolytes. The original Monroe-Newman model, which focuses on the shear strength of the separator, has some important limitations. For example, ceramic solid electrolytes, with sufficient shear modulus to prevent dendrites according to the model, suffer from defects and grain boundaries that are susceptible to dendrite penetration, demonstrating the importance of considering real rather than ideal model systems. Furthermore, even glass solid electrolytes with few or no grain boundaries suffer from dendrite penetration.[31–35] Dendrite suppression with soft separators under an external load[3] would also seem to violate its predictions.

Most of the work mentioned above has focused on the influence of local mechanical stresses at the dendrite- or micron-scale, an understanding of which is clearly necessary for analyzing growth of Li protrusions. In the Monroe-Newman calculations, the current within the typically 1–10 cubic μm at the growing protrusion is fixed. However, as we show below, because of the nature of contact between rough surfaces such as between Li metal, the cathode, and the separator, stresses caused by micron-sized asperity contact at one location can affect the stresses at many other asperity contacts in the surrounding regions. Thus, capturing the behavior of the system interaction in full is difficult with a single-dendrite-scale analysis. Spatial heterogeneity is known to play an important role in battery degradation;[10,36] however, to our knowledge, there have been no investigations of the effects of spatial heterogeneity, on a scale larger than a single dendrite, of mechanical contact stresses that are generated when a macroscopic external pressure is applied to electrodes with realistic (rough at the micron-scale) surfaces.

Theoretical work aimed at accounting for spatial heterogeneity in pressure must consider the nature of the cell architecture, including modeling the contacts for a realistically rough cathode—its porosity, generally near or above 30% for commercial cathodes, ensures that its surface is rough. A significant level of roughness is inevitable for the Li metal as well,[3,11,37–40] which adds to the complexity of the stress field.

In this work, we ask how an external pressure can inhibit dendrite growth in lithium metal batteries, even in the absence of a stiff (shear strength > 1 GPa)[20] electrolyte or separator. Our approach is to model the mechanical and associated electrochemical-mechanical interactions of a single electrode pair under experimental conditions similar to those used by Dahn et al.[3] In those experiments, a Cu foil current collector supported by a rigid structure served as the negative electrode upon which Li metal was deposited during charging. We used that work to guide our modeling because the experiment and analysis were particularly well characterized and because it showed a beneficial effect of presure, even for a thin separator whose mechanical properties would not have been expected[19,30] to inhibit dendrite growth according to the Monroe-Newman model.

*Electrochemical Society Member.
**Electrochemical Society Student Member.
[z]E-mail: qwang@northwestern.edu; sjharris@lbl.gov

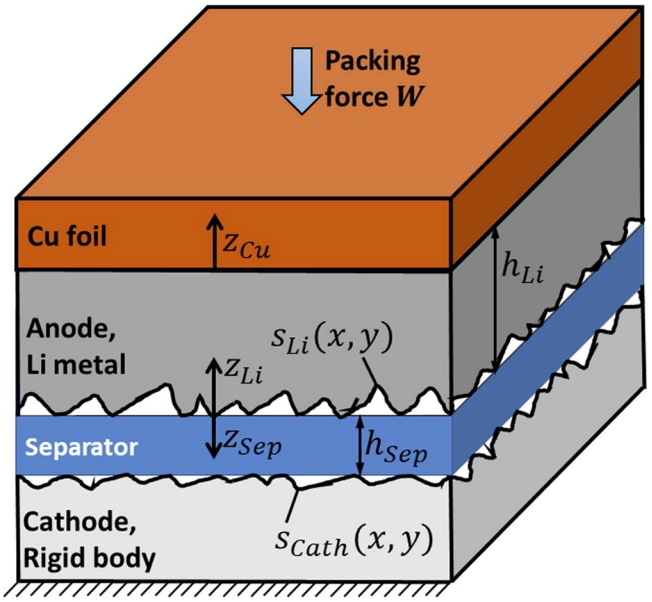

Figure 1. 3D structure of a lithium (Li) battery material system.

We consider the Li-separator and cathode-separator interfaces to be contact interfaces (where stresses are calculated), while the interface between the Cu foil and the Li metal is treated as an internal material interface. A contact interface involving rough surfaces can be modeled by using a semi-analytical method (SAM) built on core analytical solutions and supported by efficient numerical approaches, including the conjugate gradient method (CGM)[41] and the fast Fourier transform (FFT) method.[42,43] SAMs have been used for solving numerous contact problems, such as magnetoelectroelastic contacts,[44–46] elastoplastic contacts,[47–50] and contact involving rough surfaces.[51–54] Derivation of the core analytical solutions, in terms of displacements and stresses, is essential for developing a contact model and simulating the surface interactions in such structures. Here, a novel 3D Li metal-separator-cathode contact model is developed via two single interactive SAM-based analyses of single electrode pairs, aiming to properly capture the long-range effects of rough surface interations on the performance of the electrode interfaces subjected to Li elastoplastic/creep deformations and plating/stripping. This approach is then combined with an electrochemical-mechanical analysis in order to evaluate the effects of local pressure on local electrochemistry.

Formulation for 3D Contacts of Li-Separator-Cathode Interfaces

Problem description.—Figure 1 illustrates the 3D structure of a Li metal pouch cell with a single electrode pair. A liquid electrolyte fills the pores, shown in white. We assume that, since there is essentially 100% pore connectivity in commercial electrodes,[55] excess electrolyte can be locally squeezed out under any local load—ultimately, to the edges of the pouch, as is the case for gases[56]—so that for purposes of these calculations we assign a zero modulus to these regions and ignore their contribution to the local pressure, even though the pores always remain filled with electrolyte. The Poiseuille equation predicts that for a pressure differential of 1 atm, an electrolyte viscosity of 2 cp,[57] and a pore diameter of 0.1 μm, electrolyte can flow through the electrode in less than 1 second, supporting this assumption.

Rectangular Cartesian coordinates (x, y, z_{Li}), (x, y, z_{Sep}) and (x, y, z_{Cu}) are introduced with the positive z_{Li} axis oriented into the depth direction (or the vertical direction) of the Li metal, the positive z_{Sep} axis oriented into that of the separator, and the positive z_{Cu} axis oriented into that of the copper, as shown in Figure 1. The Li-separator-cathode contact problem is subject to the following considerations:

- During the charge cycle, the thickness of the Li metal increases from 2 μm to 18 μm, corresponding to an incremental 3.3 mAh.[3] Simultaneously, the external load increases. We treat the copper foil plus its supporting structure as a half space, where any effects from the far side of the supporting structure are considered as part of the fixed boundary condition. The elastic modulus of the copper foil on the rigid support is taken to be that of copper.
- The separator is treated as continuous body whose only important property is its elasticity. (See below for additional discussion.)
- We assume that the Li metal is elastic-perfectly-plastic for low-to-moderate strain rates ($<3 \times 10^{-4}$ sec^{-1}),[58] or viscoplastic subject to creep otherwise.
- The cathode is treated as a rigid body because the elastic moduli for all commercial cathode particles are much larger (>100 GPa) than those of its contact partners—a polypropylene separator (~0.22GPa[59,60]) and Li metal. The binder can be relatively soft, but we assume that the calendering process, which occurrs at high pressures before assembly, has made the cathode much more rigid (jammed) in compression than the separator and the Li metal.[61] (Calendering, a process carried out for commercial electrodes, can reduce the porosity by up to a factor of 2,[62] with the compressive forces used in calendering ultimately limited by the fracture strength of the particles.[63,64]) Our analysis assumes a calendered electrode to make it relevant to real-world systems.
- The lengths of the system, L_c in the x and y directions, are taken to be infinite relative to the separator thickness h_{Sep} (13.5 μm).
- Local contact stresses induce electrochemical overpotentials that may affect local plating.

Interfacial conditions.—*Li-Separator (Li-Sep) interfacial conditions.*—We introduce a 3D rough surface profile $s_{Li}(x, y)$ of the Li as a function of lateral coordinate variables x and y. The gap $g_{Li-Sep}(x, y)$ at the Li-Separator interface (i.e. $z_{Li} = z_{Sep} = 0$) can be calculated by considering the deformation, roughness, and morphological evolution due to Li ions plating/stripping and to Li creep,

$$g_{Li-Sep}(x,y) = u_{Li,z}(x,y,0) + u_{Sep,z}(x,y,0) + s_{Li}(x,y) - \delta_{Li-Sep} - d_{Li-creep}(x,y) + \gamma \cdot d_{Li-p/s}(x,y), \quad [1]$$

where $u_{Li,z}(x, y, 0)$ and $u_{Sep,z}(x, y, 0)$ are the surface vertical displacement components of the Li and the separator, respectively, $g_{Li-Sep}(x, y)$ is the gap between the Li and the separator, δ_{Li-Sep} is the relative rigid-body motion between Li and the separator, $d_{Li-creep}(x, y)$ is the height decrease due to Li creep effects, and $d_{Li-p/s}(x, y)$ is the height change due to Li ions plating on or stripping from the Li electrode, with $\gamma = 1$ for the charging process, and $\gamma = -1$ for the discharging process.

Mechanical contact.—Due to the roughness of the Li surface, the contact and non-contact regions at the Li-Sep interface are complementary to each other, where the contact region Γ_{Li-Sep} is subjected to contact pressure p (at the Li-Sep interface). Hence, the contact condition for pressure distributions can be written as,

$$\begin{aligned} &p(x,y) > 0 \;\&\; g_{Li-Sep}(x,y) = 0, \quad \forall (x,y) \in \Gamma_{Li-Sep}, \\ &p(x,y) = 0 \;\&\; g_{Li-Sep}(x,y) > 0, \quad \forall (x,y) \notin \Gamma_{Li-Sep}, \end{aligned} \quad [2]$$

where the overall mechanical equilibrium condition for the packing force W in the modeled region, must satisfy

$$\int_{\Gamma_{Li-Sep}} p\,(x,y)\,dxdy = W. \quad [3]$$

The surface stresses in the Li and separator at the Li-Sep interface (i.e. $z_{Li} = z_{Sep} = 0$) can be written as,

$$\sigma_{Li,zx}(x,y,0) = 0, \quad \sigma_{Li,zy}(x,y,0) = 0, \quad \sigma_{Li,zz}(x,y,0) = -p(x,y), \quad [4]$$

$$\sigma_{Sep,zx}(x,y,0) = 0, \quad \sigma_{Sep,zy}(x,y,0) = 0, \quad \sigma_{Sep,zz}(x,y,0) = -p(x,y), \quad [5]$$

where $\sigma_{zx}(x, y, 0)$ and $\sigma_{zy}(x, y, 0)$ are the surface shear stress components, and $\sigma_{zz}(x, y, 0)$ is the surface normal stress.

Li creep.—Creep plays a critical role in understanding the mechanics of Li metal.[58,65,66] Most creep work has examined more-or-less pure Li metal,[39,58,65,67–69] while the Li metal involved in electroplating is laced with SEI (solid electrolyte interphase), which might act as a hard coating or as a reinforcement. Nevertheless, we will use existing data for pure Li in the following analysis to provide a semi-quantitative picture of creep evolution of plated Li. The generalized creep law can be written as,[58,66]

$$\dot{\varepsilon}_{creep}(x, y) = A[\sigma(x, y)]^m \exp\left(-\frac{Q_c}{RT}\right), \quad [6]$$

where $\dot{\varepsilon}_{creep}(x, y)$ is the strain rate due to creep, A is a material constant, $\sigma(x, y)$ is the stress, m is the stress exponent, Q_c is the creep activation energy, R is the gas constant, and T is the absolute temperature. The importance of creep increases when longer time frames are considered.

Li plating/stripping.—Under galvanostatic control with a spatially averaged current density I, mass conservation of Li ions leads to

$$\int \left[\dot{d}_{Li-p/s}(x, y)\, dxdy\right] = I \cdot \frac{M_{Li}}{\rho F} \cdot A_{Li}, \quad [7]$$

where $\dot{d}_{Li-p/s}(x, y)$ is the rate of height change due to Li ions plating on or stripping from Li electrode, M_{Li} is the molar mass of Li, ρ is the mass density of Li, F is the Faraday constant, and A_{Li} is the cross-sectional area of the Li electrode. Local current density $i(x,y)$ may vary with location due to local overpotentials or to changes in properties of the separator, as discussed below.

Separator-Cathode interfacial conditions.—Surface roughness was measured for a commercial $LiFePO_4$ (LFP) cathode harvested from a dry A123 20Ah pouch cell using a Bruker Dektak XT Stylus Profilometer. We take this surface to be representative of commercial, calendered[61] cathodes. A 1000μm x 1000μm region was interrogated with a 1 μm spacing, averaging over any structures at the sub-micron scale to study interactions at the sub-mm scale. The surface profile is considered as a 3D function of lateral coordinate variables x and y, i.e. $s_{Cath}(x, y)$. In the presence of a packing force W, the cathode surface asperities penetrate into the separator, deforming it. The vertical displacement $u_{Sep,z}$ of the separator at the Sep-Cath interface (i.e. $z_{Sep} = h_{Sep}$) can be written as,

$$u_{Sep,z}(x, y, h_{Sep}) = -s_{Cath}(x, y) + g_{Sep-Cath}(x, y) + \delta_{Sep-Cath} + d_{SE}, \quad [8]$$

where $g_{Sep-Cath}(x, y)$ is the gap between the separator and the cathode, and $\delta_{Sep-Cath}$ is the relative rigid-body motion between the separator and cathode, d_{SE} is the uniform volumetric change of the cathode.

Due to the roughness of the cathode surface, contact and non-contact regions in the Sep-Cath interface are complementary, where the contact region $\Gamma_{Sep-Cath}$ is subjected to a deformation constraint q (caused by cathode asperities). Hence, the contact condition for deformation constraints q can be written as,

$$\begin{aligned} q(x, y) = s_{Cath}(x, y) - \delta_{Sep-Cath} \;\&\; g_{Sep-Cath}(x, y) = 0, \\ \forall (x, y) \in \Gamma_{Sep-Cath}, \\ q(x, y) = 0 \quad \&g_{Sep-Cath}(x, y) > 0, \quad \forall (x, y) \notin \Gamma_{Sep-Cath}. \end{aligned} \quad [9]$$

Due to the lack of bonding at the Sep-Cath interface (i.e. $z_{Sep} = h_{Sep}$), the shear stresses on the separator at the Sep-Cath interface vanish,

$$\begin{aligned} \sigma_{Sep,zx}(x, y, h_{Sep}) = 0, \\ \sigma_{Sep,zy}(x, y, h_{Sep}) = 0. \end{aligned} \quad [10]$$

The overall mechanical equilibrium condition for the normal stress at the Sep-Cath interface must satisfy

$$\int_{\Gamma_{Sep-Cath}} \left|\sigma_{Sep,zz}(x, y, h_{Sep})\right| dxdy = W. \quad [11]$$

Li-Cu interfacial conditions.—Following the experiments of Dahn et al.,[3] we assume an initial 2 μm thick Li film that is perfectly bonded to the Cu; Li metal is added during the charge step. Displacements at the Li-Cu interface (i.e. $z_{Li} = h_{Li}$ and $z_{Cu} = 0$) are

$$\begin{aligned} u_{Li,x}(x, y, h_{Li}) = u_{Cu,x}(x, y, 0), \\ u_{Li,y}(x, y, h_{Li}) = u_{Cu,y}(x, y, 0), \\ u_{Li,z}(x, y, h_{Li}) = u_{Cu,z}(x, y, 0), \end{aligned} \quad [12]$$

Displacement and stress solutions.—The boundary-value problem described by Eqs. 1–12 can be handled by a fast Fourier transform (FFT)-based numerical process, if the Fourier-transformed solutions of displacements and stresses at the Cu-Li and the separator-rigid cathode systems are analytically solvable.

The Fourier-transformed elastic displacements and stress solutions for the Cu-Li metal system can be found in Ref. 43, also provided in the Supplementary Information S1. The Fourier transformed displacements and stresses for the separator-rigid cathode system can be obtained starting from the Lamé-Navier equations using the Papkovich–Neuber potentials and by considering the interfacial conditions Eqs. 5, 8–10. Solutions and derivation details are also presented in the Supplementary Information S2.

FFT-based elastic-perfectly-plastic contact modeling.—In the FFT-based numerical process, the contact information (e.g. pressure, contact stress) and profiles of the Li and cathode surfaces are taken as discrete data from an infinite sequence along the x and y directions. A representative portion, $L_c \times L_c$, in the $x - y$ plane is selected as the physical domain, assuming that $L_c \times L_c$ is one period of the whole structure, as shown in Figure 2. This means the overall information, including surface features, loading conditions, and mechanical behaviors, are taken as periodically repeated from those in the representative $L_c \times L_c$.

To operate the FFT-based algorithm, the solutions in Displacement and stress solutions section need to be obtained in the form of frequency response functions (FRFs) by the continuous convolution and FFT (CC-FT) algorithm.[70] Details of CC-FT algorithm are given in Supplementary Information S3. The contact simulation was written in Fortran, involving the CC-FT algorithm[70] and the conjugate gradient method (CGM).[41] The details of the contact algorithm and a flow diagram are given in Supplementary Information S4.

In most elastic-perfectly-plastic contact models involving rough surfaces, when yield occurs at the surface of materials, we can simply truncate the contact pressure peaks at the material hardness, which is typically (depending on the sample geometry) about 3 times the yield strength σ_Y. (Hardness, a measure of resistance to plastic deformation from indentation, is higher than the yield strength in tension because subsurface material must be pushed out of the way.) As shown in Ref. 71, the accuracy of the pressure calculation when using such a truncation treatment increases with decreasing material yield strength, indicating that truncation for Li, which has a low yield strength, should be acceptably accurate.

In the following numerical computation, the physical representative domain of $L_c \times L_c$ was discretized with a 400×400 subset grid in the x and y directions, where the periodic length of the modeled interface is set to $L_c = 400$ μm, and the spatial resolution is 1 μm. At this size, the major features of the surface are included, and CPU times for our time-dependent 3D calculations are reasonable.

To calculate the Li subsurface stresses, the Li was discretized with 200 grid points in the z direction. The spacing of these grid points depended on the subsurface stress gradients. The macroscopic external pressure is calculated by $P = W/(L_c \times L_c)$ where W is the total packing force applicable to this representative domain.

Experiment shows that under low pressures, plated Li can be porous,[3,13] while deposition at higher pressure can lead to a denser material. In the Dahn et al. pressurized experiments,[3] run at a current density of 0.6 mA/cm^2 (corresponding to roughly 3 μm Li per hour), a Li metal thickness increase of ~250μm was measured during deposition in their multi-electrode-pair cell, compared to a calculated

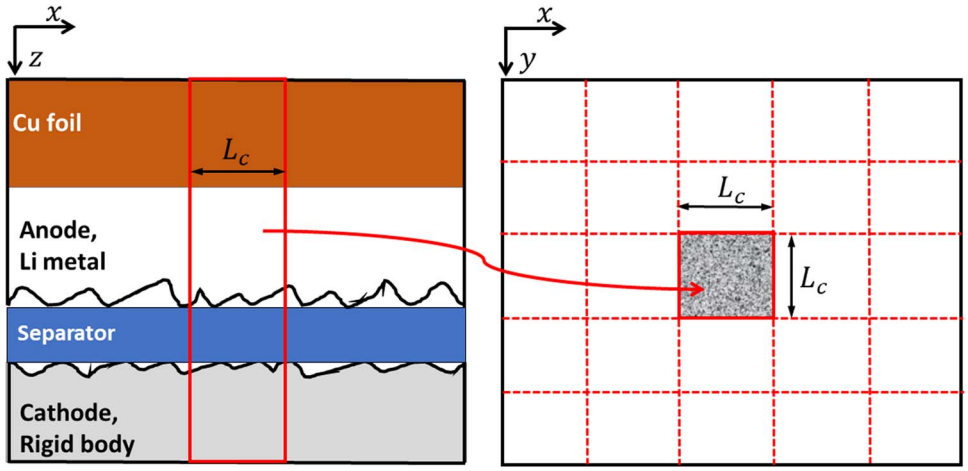

Figure 2. Illustration of a representative portion of the Cu-Li-separator-cathode layers, $L_c \times L_c$.

thickness increase of 254μm. This calculation explicitly assumed that the plated Li was fully dense at 0.534 g/cm^3. (No account was taken of any volume change in their cathode, but we have measured the crystallographic volume change of their cathode material to be less than 1% upon delithiation.[72]) The agreement, to within about 2% between the calculated and measured thickness increase, argues that the plated Li in their high-pressure experiments was reasonably close to fully dense.

There is considerable discussion in the literature over the appropriate value to use for the compressive yield strength of Li metal. Low values for bulk Li have been measured[73,74] in the range of 0.41 to 0.89 MPa. However, more recent work has found that the compressive yield strength depends strongly on the size of the Li structure,[67,68] with a value of 100 MPa reported for 1μm features. Furthermore, Janek et al.[75] have shown that the interface resistance between Li metal and a solid electrolyte decreases inversely pressure to at least 41 MPa, suggesting a hardness at least that high with a corresponding yield strength greater than 13 MPa. In the absence of definitive yield strength data, we have performed calculations for the three yield-strength values, 0.66, 10, and 100 MPa, shown in Table I, to consider a wide range of possible Li performances. By covering this range, we also take into account an increase in yield strength of Li due to the presence of SEI[76] or other impurities (see below).

Results and Analysis

Model properties and verification.—The cathode surface profile is shown in Figure 3a. As expected, the measured roughness of this commercial (calendered) electrode is relatively low. The surface roughness of Li metal varies dramatically,[37] within each cycle and from cycle to cycle, and it can include protrusions formed during charge as well as voids formed during discharge.[39,40] Rather than trying to capture the full range of possible Li surfaces in our calculations, we will consider 2 cases: a perfectly smooth Li surface and a surface with a sinusoidal form, $s_{Li}(x, y) = A_0 \cos(2\pi x/\lambda)\cos(2\pi y/\lambda)$, where we have taken $A_0 = 1.0\mu$m and $\lambda = 40\mu$m, Figure 3b, as an example. Each peak may be considered as a model Li protrusion (incipient dendrite); each valley may be considered as a model void. We believe that by analyzing simple surfaces, we can obtain a semi-quantitative understanding of local stresses and their distributions for a range of realistic conditions.

When the separator thickness h_{Sep} approaches infinity, the coefficients in Eq. (S2.16) become $C = -1/\alpha$, $\bar{C} = 0$, $D = (1 - 2\nu_{Sep})/\alpha^2$, and $\bar{D} = 0$. Therefore, the Fourier-transformed displacement in Eq. (S2.8) yields $\tilde{u}_{Sep,z} = (1 - \nu_{Sep})\tilde{p}/(\mu_{Sep}\alpha)$, which is identical to the classical solutions to a half-space given in Ref. 42, confirming that the Fourier-transformed solutions with their coefficients Eqs. (S2.6-S2.14, S2.16) are correctly calculated for this case. To further verify the CC-FT based numerical modeling, we compared the term, $\delta_{Sep-Cath} - u_{Sep,z}$ (ignoring the volumetric change of the cathode, which is less than 1%),[72] at the separator-cathode interface with the cathode surface profile, s_{Cath}, of Figure 3a, for the problem of a large macroscopic external pressure $P = 1,585$kPa, a Li thickness $h_{Li} = 18\mu$m, and the Li surface profile s_{Li} of Figure 3b. For such a large external pressure, the calculation led to no gap between the separator and the cathode. As shown in Figure 3c, $\delta_{Sep-Cath} - u_{Sep,z}$ calculated from the present numerical model agrees well with the surface profile s_{Cath}. Figure 3c simply indicates that the results of our calculation are consistent with the interfacial condition given in Eq. 8.

Contact stress calculation.—We first calculate the Li contact stress under loading conditions during cell operation. This section focuses on static contact without considering Li creep during charging and discharging processes. In effect, we are considering here the case when microstructure changes due to creep are slow compared to those due to deposition. An analysis for the case when creep and deposition occur at comparable rates is provided in Creep of Li section below.

Smooth Li.—Figures 4 and 5 plot the Li surface stress contours ($x - y$ section), and Li subsurface von Mises stress contours ($y - z$ section) for smooth Li surfaces with assumed yield strengths of $\sigma_Y = 0.66$MPa, 10MPa and 100MPa. In both figures, the presence of local contact is due to the roughness effect of the cathode surface transmitted through the separator. In the experiments,[3] the packing pressure increased with Li thickness h_{Li}, and we modeled 3 cases taken from their Table I, where $(P,\ h_{Li}) = (744$ kPa, 2μm), (1, 205 kPa, 11μm), and (1, 585 kPa, 18μm). Our calculation results show no gaps between the separator and the cathode at these high pressures, which means their surfaces are conformal, and the entire separator-cathode interface carries load. On the other hand, the Li-separator interface is not conformal. Red, green, and yellow regions in Figures 4a and 5a show areas where there is contact between the separator and the Li, while the blue regions denote regions where the stress is zero (no contact). Figure 5c shows the gap thickness between the Li and the separator where white regions show where the gap is zero, denoting the contact areas. The maximum gap is between 0.5 and 0.6 microns for the case of $(P,\ h_{Li}) = (744$kPa, 2μm). The gap

Table I. Material properties of lithium metal, polypropylene separator and copper.

	Lithium	Separator	Copper
Elastic modulus E [GPa]	7.82[69]	0.22[59]	100
Poisson's ratio ν	0.381[66]	0.4	0.33
Yield strength σ_Y [MPa]	0.66,[58] 10, 100[67]	-	-

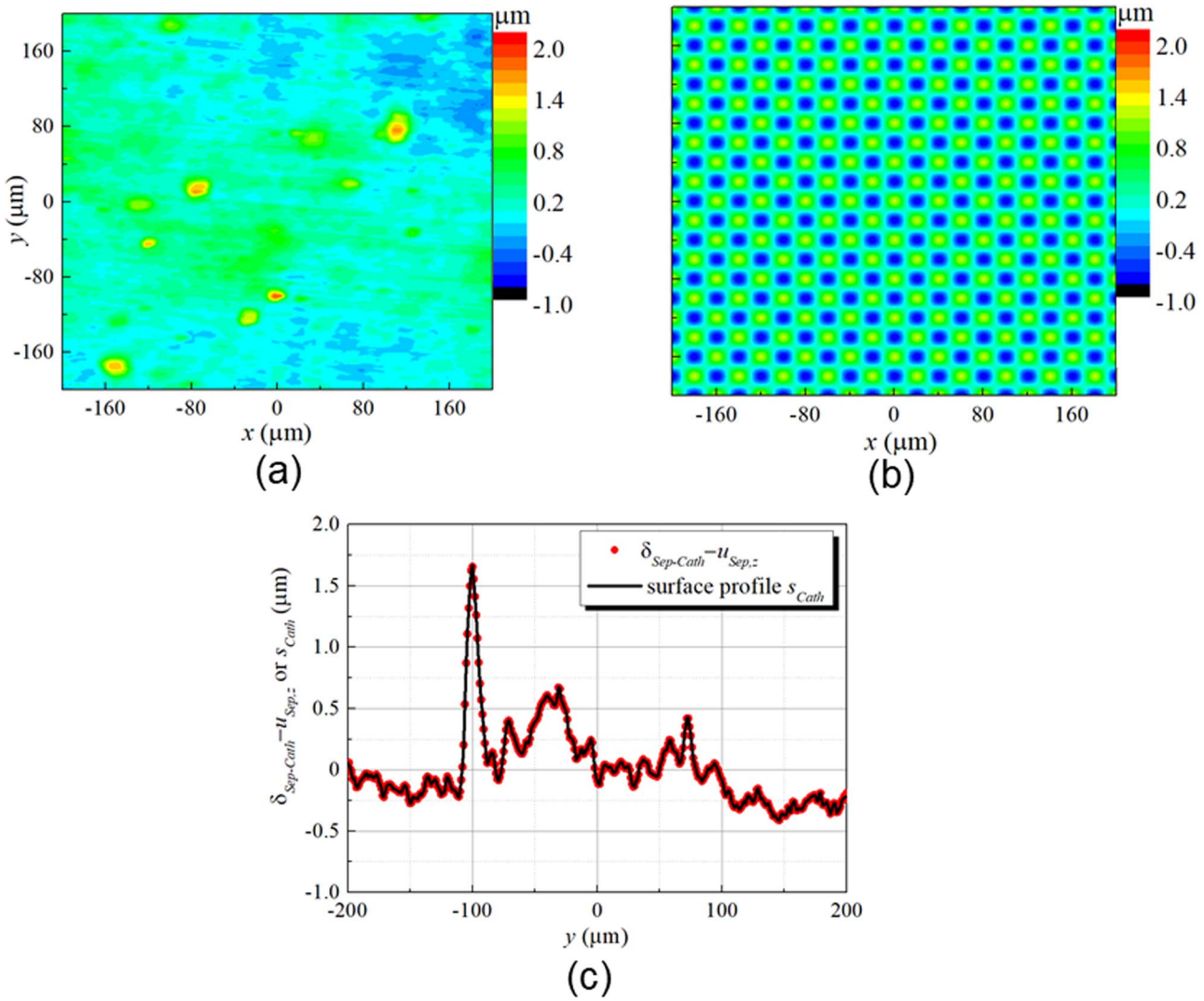

Figure 3. (a) Contour map of the measured cathode surface height distribution, s_{Cath}; (b) generated sinusoidal height pattern for the Li metal surface s_{Li}; (c) comparison of the term, $\delta_{Sep-Cath} - u_{Sep,z}$, calculated from the present numerical modeling with the cathode surface profile s_{Cath} along the y direction at $x = 0$, supporting the validity of the Sep-Cath interface model.

volumes are 2×10^4, 1.3×10^4, and 9×10^3 μm^3, for $(P, h_{Li}) =$ (744kPa, 2μm), (1, 205kPa, 11μm), and (1, 585kPa, 18μm), respectively. For the low yield stress case, the surface stress reaches its maximum value of 1.98MPa, which is $3\sigma_Y$, at most contact points. The von Mises stress values indicate that subsurface regions below the contact points are plastically deformed.

For a yield strength of $\sigma_Y = 10$MPa, possibly corresponding to that for the Li structures near 10 μm[67] or for Li with a hard coating such as an SEI,[77] the fraction of the area in contact A_p is reduced because the larger yield strength allows contact asperities to carry more load. The peak surface stress for this case is 25 MPa, below its maximum value of $3\sigma_Y = 30$MPa. The peak von Mises stress is 6.66 MPa, lower than the yield strength, so that no plastic yielding occurs inside the Li metal. Peak von Mises stress for the case of yield strength $\sigma_Y = 100$MPa (1 μm Li structures) are identical to those for $\sigma_Y = 10$MPa.

Rough Li.—Figures 6, 7, and 8 plot the Li surface stress contours ($x - y$ section), and Li subsurface von Mises stress contours ($y - z$ section) for the "rough" (i.e., sinusoidal with an amplitude of 1 μm) Li surface of Figure 3b. For the low yield strength case, $\sigma_Y = 0.66$MPa, the surface stress either reaches its maximum value of 1.98MPa or is 0. Most of the subsurface Li below the contact points is plastically deformed, highlighted by red regions. The surface and sub-surface stresses for $\sigma_Y = 10$MPa, Figure 7, are plastic only near some of the contact points. For $\sigma_Y = 100$MPa, Figure 8, the contact points can carry larger loads without plasticity. The largest surface stress is 40 MPa, too low for plastic deformation. These results show that Li protrusions (incipient dendrites) are exposed to significant compressive contact stresses (up to tens of MPa) by the time they are only 1 μm tall.

Figure 9 shows how the smooth (a) and sinusoidal (b) Li surfaces deform against the cathode for external pressures of $P = 744$, 1,205, and 1,585 kPa. The cathode surface profile along the y direction (for $x = 0$) from Figure 3a is also plotted as a dotted line in Fig. 9a for comparison. For a smooth Li surface, asperity peaks of the rigid cathode surface penetrate into the separator, as described by interfacial condition Eq. 6. As expected, corresponding convex crests appear on the separator surface at the Li-separator interface. For the sinusoidal surface, direct contacts between the Li asperities and separator become stronger, so that the Li stress distribution is dominated by details of the Li surface profile in this example.

Lighter loads.—The previous calculation results show that for an external pressure of $P = 744$ kPa or greater, the cathode surface is completely conformal with the soft separator. Figure 10a plots the surface contact stresses on Li for lighter external pressures of

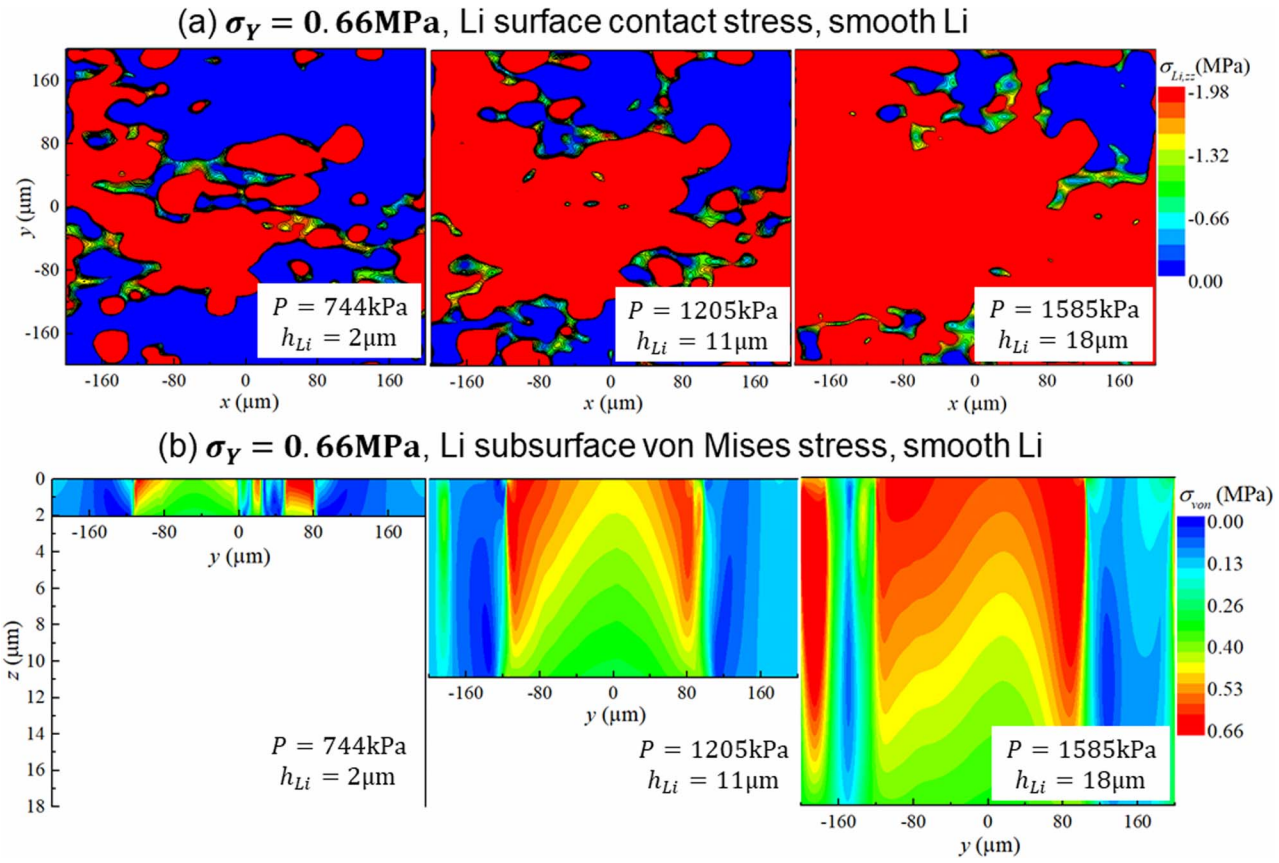

Figure 4. (a) Surface stress contours in Li, and (b) subsurface von Mises stress contours at $x = 0$ in Li, for Li yield strength $\sigma_Y = 0.66$MPa under various external pressures and Li thicknesses (P, h_{Li}) = (744kPa, 2μm), (1205kPa, 11μm), and (1585kPa, 18μm), for the cathode surface shown in Figure 3a and a smooth Li surface.

$P = 100$, 200, and 300 kPa, and a Li thickness of $h_{Li} = 10\mu$m. For such pressures, which may be of practical interest, there are gaps between the separator and cathode, shown in red, green, blue and yellow regions in Figure 10b. Separator-cathode gap maps for the rough Li case are identical to those for smooth Li case. Figure 11 plots the fraction of the area in contact as a function of the external pressure, for both the Li-separator and separator-cathode interfaces. When the external pressure is 500kPa, the whole cathode interface is in contact with the separator, while only 12.6% of the Li is in contact with the separator.

Important properties of the separator.—We first point out two important properties of the separator. (1) Although we are treating the separator as a homogeneous solid, in fact it is heterogeneous, with pores that penetrate through it. The smaller in-plane dimension of the pores is typically about 100 nm[78] or less,[60] ~2 orders of magnitude smaller than the contact regions seen in Figure 5. Thus, from a mechanical point of view, treating the separator as homogeneous is a reasonable approximation at the scale of interest here. (2) Assuming that all of the separator pores are open and filled with electrolyte, Li^+ ions can diffuse through open separator pores for purposes of plating or stripping just as readily in contact regions as in non-contact regions (but see discussion below).

Our calculations show that the macroscale interactions studied here tend to distribute the load in complex patterns that depend on the surface roughness of the electrodes at a sub-mm scale These stress fields do depend on mechanical properties of the separator, but in a manner different from that discussed by Monroe and Newman.[19,29,30]

Our analysis of the microscopic stresses at sub-mm length scales shows that even under high packing forces, most of the Li metal surface is not in contact with the separator (unless we use the low[67,68] Li yield strength of <1 MPa together with very high pressures). We note that previous work has assumed, implicitly or explicitly, that contact between the separator and the lithium metal is largely or perfectly conformal, so that any protrusion that starts to form on charge could immediately be subject to being "squashed" by a "stiff" separator. Whatever the validity of this picture at micron or sub-micron scales, our results indicate that the mechanics involved in pressurizing a Li metal cell should also take larger scales into account.

The primary question we must ask with respect to our analysis is: In the absence of a stiff separator,[19] and in the absence of physical contact over most of the Li surface (Figure 5), how can we understand the experimental observation that an external pressure can impede growth of Li protrusions over the full surface? We will offer hypotheses that may, singly or in combination, explain the observations. We will also propose possible experimental tests of these hypotheses.

Asperities.—Our calculations show that stresses at asperity contacts can exceed the average (macroscale) pressure by as much as 2 orders of magnitude, if we use the recent measurements for the yield strength[67,68] (see below for the effects that SEI may have on the yield strength). We expect that Li ions will tend to avoid plating in regions with such high stresses because an incremental Li atom deposited on the surface of a region under load is at higher energy than one deposited on a surface that is not feeling any load. In general, depositing on the regions that are supporting the external load requires $P\Delta V$ mechanical work to displace the cathode surface there (by 15.9 microns in this case).[79]

To evaluate the impact of pressure on deposition rate, we evaluate the Butler-Volmer equation:[29,80]

$$i_{BV} = i_o\left[\exp\left(\frac{F\eta}{2RT}\right) - \exp\left(-\frac{F\eta}{2RT}\right)\right] \qquad [13]$$

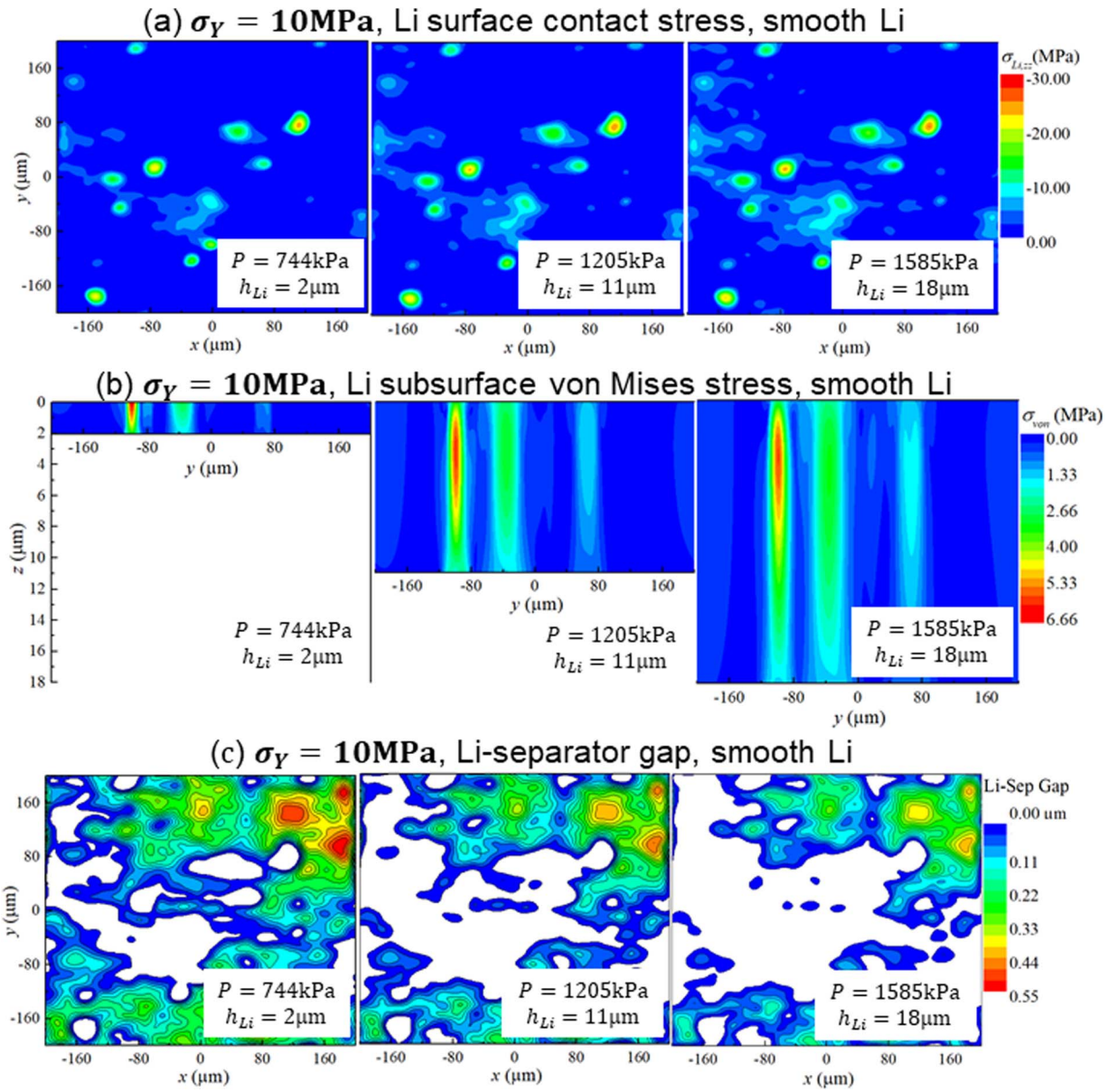

Figure 5. (a) Surface normal stress contours on Li, and (b) subsurface von Mises stress contours in Li, for Li yield strength σ_Y = 10MPa under various external pressures and Li thickness (P, h_{Li}) = (744kPa, 2μm), (1205kPa, 11μm), and (1585kPa, 18μm), for the cathode surface shown in Figure 3a and a smooth Li surface. Results for a yield stress of 100 MPa are identical. (c) Gap contours between the Li and the separator. Only the white regions are in contact.

where i_{BV} is the local reaction rate,

$$i_o = i_{o,ref} \exp\left(\frac{\Delta\Phi}{2RT}\right) \quad [13a]$$

is the effective exchange current density, $i_{o,ref}$ is the reference exchange current density, R is the gas constant, F is Faraday's constant, $\Delta\Phi$ is the change in the electrochemical potential due to pressure effects, and η is the (transport related) overpotential. Because of the relatively wide aspect ratio of features (low curvature) and low shear modulus of the separator/electrolyte, we simplify Equation 9 of Ref. 80 to:

$$\Delta\Phi = \frac{1}{2F}\left(\bar{V}_{Li} - (1 - t_{Li^+})\,\bar{V}_{elec}\right)\Delta p_{Li} \quad [14]$$

where $\bar{V}_{Li}$ and $\bar{V}_{elec}$ are the partial molar volumes of lithium and electrolyte, t_{Li^+} is the transferrence number, and Δp_{Li} is the pressure on the lithium surface.

For conditions shown in Figures 5 and 7 (σ_Y = 10 MPa), the maximum surface pressure is near 30 MPa, for smooth or rough surfaces. Using parameters from Ref. 80, 30 MPa of pressure equates to a potential change of 16 mV. While this may seem small, it reduces the effective exchange current density by 27%. This lower reaction rate in the high pressure regions will preferentially lead to higher plating in low pressure regions, smoothing out deposition patterns.

We conclude that for assumed intermediate-to-high Li yield strength values, there is a tendency for Li to plate in unstressed regions (non-contact regions), ultimately allowing the most-stressed regions to partially unload. On the other hand, for low Li yield strength values or under conditions where the overpotential is sufficiently small, the rate of height change $\dot{d}_{Li-p/s}$ in Eq. 7, can be approximated as,

$$\dot{d}_{Li-p/s} = I \cdot \frac{M_{Li}}{\rho F} \cdot \frac{L_c \times L_c}{1 - A_c}, \quad [15]$$

where L_c is the cell length, and A_c is the contact area.

Creep of Li.—For moderately fast deposition rates, creep and deposition should be considered simultaneously. Because the contact

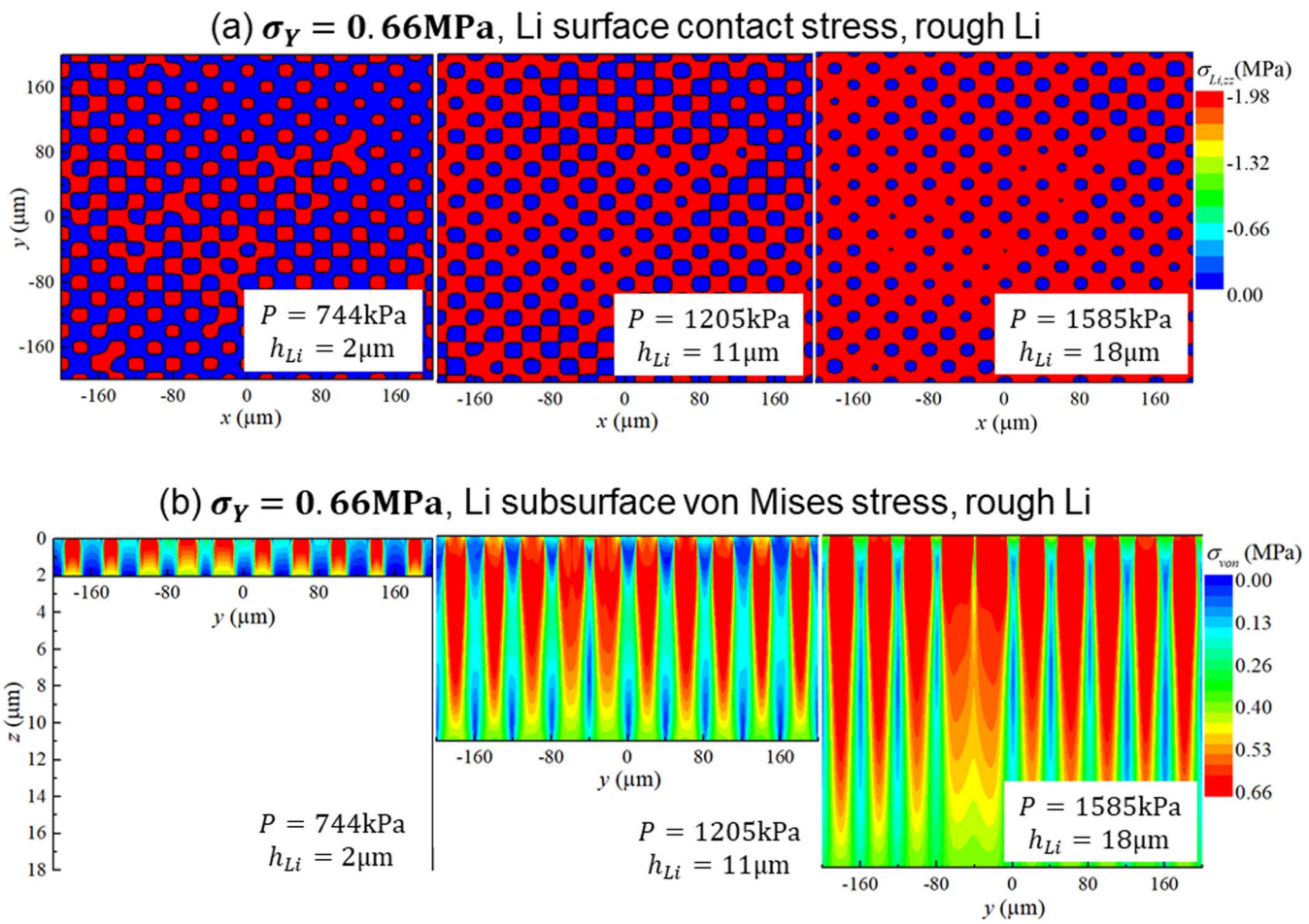

Figure 6. (a) Li surface stress contours, and (b) Li subsurface von Mises stress contours, for Li yield strength $\sigma_Y = 0.66$MPa under various loading groups of external pressures and Li thickness $(P,\ h_{Li}) = (744\text{kPa}, 2\mu\text{m})$, $(1205\text{kPa}, 11\mu\text{m})$, and $(1585\text{kPa}, 18\mu\text{m})$, for the cathode surface shown in Figure 3a and the Li surface in Figure 3b.

pressure is non-uniformly distributed at the Li/Separator interface, the strain rate in Eq. 6 is also non-uniformly distributed, and we assume that only the contact region is subjected to creep effects.

The dynamics of deformation due to rough asperites is quite different from that described by the uniaxial creep law Eq. 6; a depth-sensing indentation creep test is required. As suggested in Ref. 81, the rate of height loss due to creep, $\dot{d}_{Li-creep}$, under indentation loadings can be expressed as,

$$\dot{d}_{Li-creep}(x,y) = \dot{\varepsilon}_{i-creep}(x,y) \cdot u_{Li,z}(x,y), \quad [16]$$

where $u_{Li,z}(x,y)$ is the vertical deformation of Li metal. In order to use the creep law Eq. 6, we need to modify the creep data obtained from uniaxial tests. As suggested in Ref. 82, the relationship between strain rates measured with uniaxial $\dot{\varepsilon}_{u-creep}$ and indentation tests $\dot{\varepsilon}_{i-creep}$ is

$$\dot{\varepsilon}_{i-creep}(x,y) = \alpha \cdot \dot{\varepsilon}_{u-creep}(x,y), \quad [17]$$

while the relationship between the uniaxial stress and contact pressure is

$$p(x,y) = \beta \cdot \sigma(x,y), \quad [18]$$

where α and β are Bower factors, which are set to $\alpha = 0.128$ and $\beta = \sigma_Y/0.7982$, according to Refs. 65,82,83.

Using Eq. 6, the rate of height loss due to creep, $\dot{d}_{Li-creep}$, can be expressed as,

$$\begin{aligned}\dot{d}_{Li-creep}(x,y) &= 0.128\,A\left[\frac{0.7982p(x,y)}{\sigma_Y}\right]^{6.6}\exp\left(-\frac{Q_c}{RT}\right)\cdot u_{Li,z}(x,y)\\ &= 10^{-4}\,A\left[\frac{2.3597p(x,y)}{\sigma_Y}\right]^{6.6}\exp\left(-\frac{Q_c}{RT}\right)\cdot u_{Li,z}(x,y),\end{aligned} \quad [19]$$

In our work, we choose the stress exponent $m = 6.6$, $A\exp(-Q_c/RT) = 0.01\text{MPa}^{-m}s^{-1}$ for $T = 298$K from Ref. 58. The factor 10^{-4} is identical to the strain decay observed in Ref. 66 and used for calculation in Ref. 84.

We analyzed creep during 5-hour charges using current densities of $I = 0.05,\ 0.2$, and 0.3mA/cm^2. We updated the Li morphological profile in Eq. 1 by the rate of height increase from Eq. 15, and the rate of height loss due to creep Eq. 19, based on the contact pressure and gaps of each incremental time step of 6s. Figure 12 shows the fraction in Li-separator contact for constant packing pressure $P = 500,\ 1,000$, and $2,000$kPa. Figure 13 plots the fraction in Li-separator contact for a packing pressure varying in 0–2,000kPa. There is a competition between loss of height due to creep and height gain from electroplating. When these rates are similar, the calculated contact area becomes unstable, as can be seen for $P = 500$kPa and current densities $I = 0.2$ and 0.3mA/cm^2. Thus, if dendrite growth is fast compared to characteristic creep times, then creep does not play a significant role in bringing the system toward equilibrium where surface features tend to be leveled. Similarly, a small local overpotential can hardly prevent local deposition at high current densities. Moreover, the higher the required current density is, the higher the packing pressure must be for stable Li surface developments in plating/striping. For the cases analyzed, P ≥ 1 MPa is needed.

It deserves re-emphasizing that the processes discussed above can hardly be captured unless stress heterogeneity at greater-than-dendrite-scale is recognized and multiple asperity interactions are analyzed in the Li-separator-cathode sandwich structure.

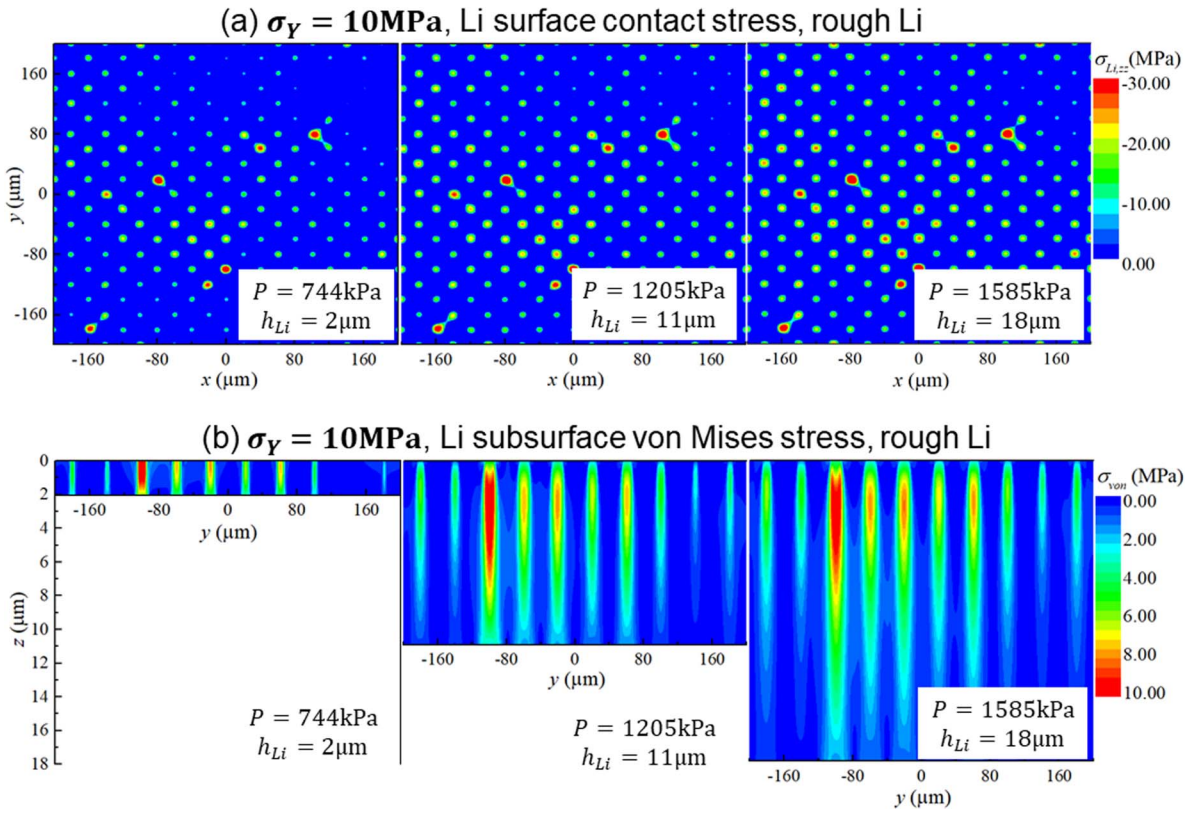

Figure 7. (a) Li surface stress contours, and (b) Li subsurface von Mises stress contours, for Li yield strength σ_Y = 10MPa under various loading groups of external pressures and Li thickness (P, h_{Li}) = (744kPa, 2μm), (1205kPa, 11μm), and (1585kPa, 18μm), for the cathode surface shown in Figure 3a and the Li surface in Figure 3b.

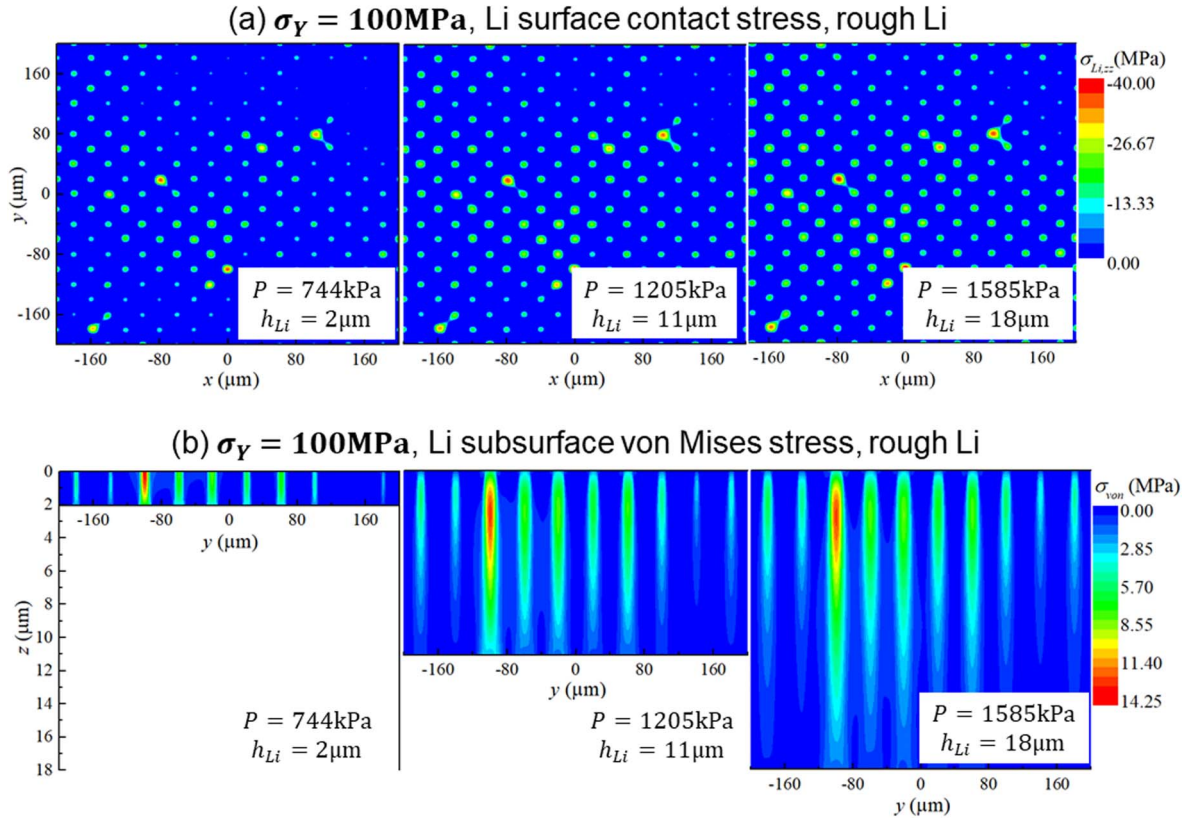

Figure 8. (a) Li surface stress contours, and (b) Li subsurface von Mises stress contours, for Li yield strength σ_Y = 100MPa under various loading groups of external pressures and Li thickness (P, h_{Li}) = (744kPa, 2μm), (1205kPa, 11μm), and (1585kPa, 18μm), using the cathode surface shown in Figure 3a and the Li surface in Figure 3b.

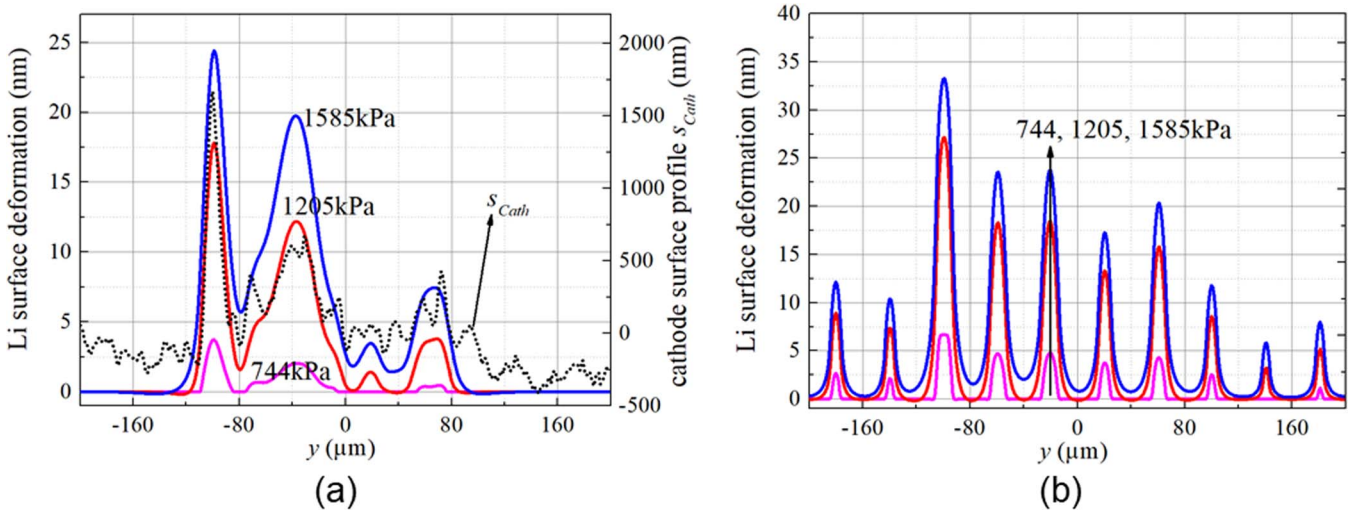

Figure 9. Li surface profile along the y direction for $x = 0$ and for different external pressure $P = 744$, 1205, and 1585 kPa, (a) for smooth Li surface to the case of Figure 5a, and (b) for rough Li surface to the case of Figure 7a. The cathode surface profile along the y direction is also plotted in Figure 9a for comparison.

Discussion

Additional consequences of the present picture.—Up to now, our analysis indicates that mechanical forces and subsequent creep will tend to homogenize the stress field and flatten the Li, but only until the stress effects at asperities become small compared to the factors that enhance dendrite growth,[11] at which point this mechanism will no longer operate. Conversely, new protrusions may form and grow during plating, leading to new asperity contacts, unless the stresses there become so high that plating moves elsewhere. This picture differs qualitatively from the Monroe-Newman model in that we are not focusing on properties of the separator that are needed to prevent local dendrite lengthening, and we are not specifying a particular local current density. Instead, we are focusing on longer-range heterogeneity in local contact stresses that encourages a more uniform Li plating as the current density redistributes to regions that may be far away from any individual protrusion under stress.

We next address the possibility that protrusions could grow as nanoscale dendrites through the separator pores. There is evidence that at these modest current densities (well below the limiting current), dendrite growth through nanoscale pores does not occur. Monroe and Newman's Figure 12[19] shows that the dendrite radius is larger than 1 micron at the low current densities studied here, compared to the pore sizes of 0.1 microns or less in the separator. Supporting their calculation, TEM images show[14] that incipient dendrites quickly attain a tip radius of curvature greater than 1 micron. Cui et al.[85] found that Li deposited directly under a separator has a large radius of curvature. Additionally, Bazant et al.[11] showed that the tips of mossy lithium, the form that grows at low current densities, have large radii of curvature. Most important, they showed that mossy dendrites do not penetrate small pores, although their work did not involve any external pressure. In order to test our asperity picture, we suggest performing a ^{6}Li-^{7}Li isotope experiment using TOF-SIMS,[86,87] where ^{6}Li is deposited under pressure on a ^{7}Li substrate. To the extent that asperity contact stress plays a role and that separator pores can be ignored, we should see an initial (before all of the gaps have been filled) patchy surface spatial distribution of ^{6}Li and ^{7}Li that at least statistically resembles a contact stress map analogous to Figure 5.

We expect that creep can play an essential role in determining Li morphology for time scales much longer than minutes.[58] Once a mechanical situation such as that shown in Figure 5 is created, Li metal will begin to creep away from regions of high stress to regions of low stress during intervals such as after charging but before discharging, or even during charge. This possibility can be tested by rapidly charging multiple cells under identical electrochemical but various pressure conditions. The cells can then be held at rest, opened at appropriate intervals, and examined ex-situ to see if the Li surfaces have flattened (relaxed) with time in a statistical sense.

Experiment shows that growth of Li protrusions/dendrites depends on electrolyte chemistry.[3,85,88,89] A plausible contributing factor, we suggest, is that the relatively stiff SEI films could coat the Li metal or act as a reinforcement forming a Li/SEI composite. In either case, the plated Li would have a higher yield stress (overpotential) and lower creep rates compared to pure Li. This effect has been observed by Cheng et al.[76] Since SEI mechanical properties likely vary for different electrolytes, significant effects of electrolyte chemistry on dendrite growth can be expected. In addition, temperature could be expected to play an important role in the composition and properties of SEI, perhaps explaining the increased coulombic efficiency obtained at 60°C in ether solutions compared to the results at room temperature.[90] We note that high temperatures can also be achieved at current densities near 15 mA/cm^2, 25 times higher than for our model.[91] However, these high temperature results may not directly relate to the room temperature experiments modeled here.[3]

Approximations, assumptions, and limitations.—Our calculations are subject to a number of approximations, assumptions, and limitations, some of which are discussed here.

Viscoelastic and viscoplastic deformation of the separator.—Viscoelastic and viscoplastic deformation of the nanoporous polypropylene separator may further enhance the effective flattening of the Li-separator interface and corresponding uniformity of stress state. This is because the creep deformation of the separator may collapse the pore network, inhibiting ion transport through the separator in high stress regions, while enhancing plating in contact-free or low-stress locations. Such an effect has been documented in conventional Li-ion batteries and has been suggested as a mechanism for mechanically-induced capacity fade.[59,92–96] Indeed, scanning electron images of stress-induced separator pore collapse show that the collapse is spatially heterogeneous – an effect that may be attributable to the heterogeneous asperity contact. Such behavior could be confirmed with two complementary experiments: (1) a rigid counter surface (e.g. sapphire) with different levels of surface roughness (from polishing or from lithography), can be loaded against separators and the subsequent spatial pore density can be measured via a scanning electron microscope as in Ref. 92; and (2) a separator can be uniformly compressed to achieve various fractions of collapse, and its ionic transport properties can be measured.

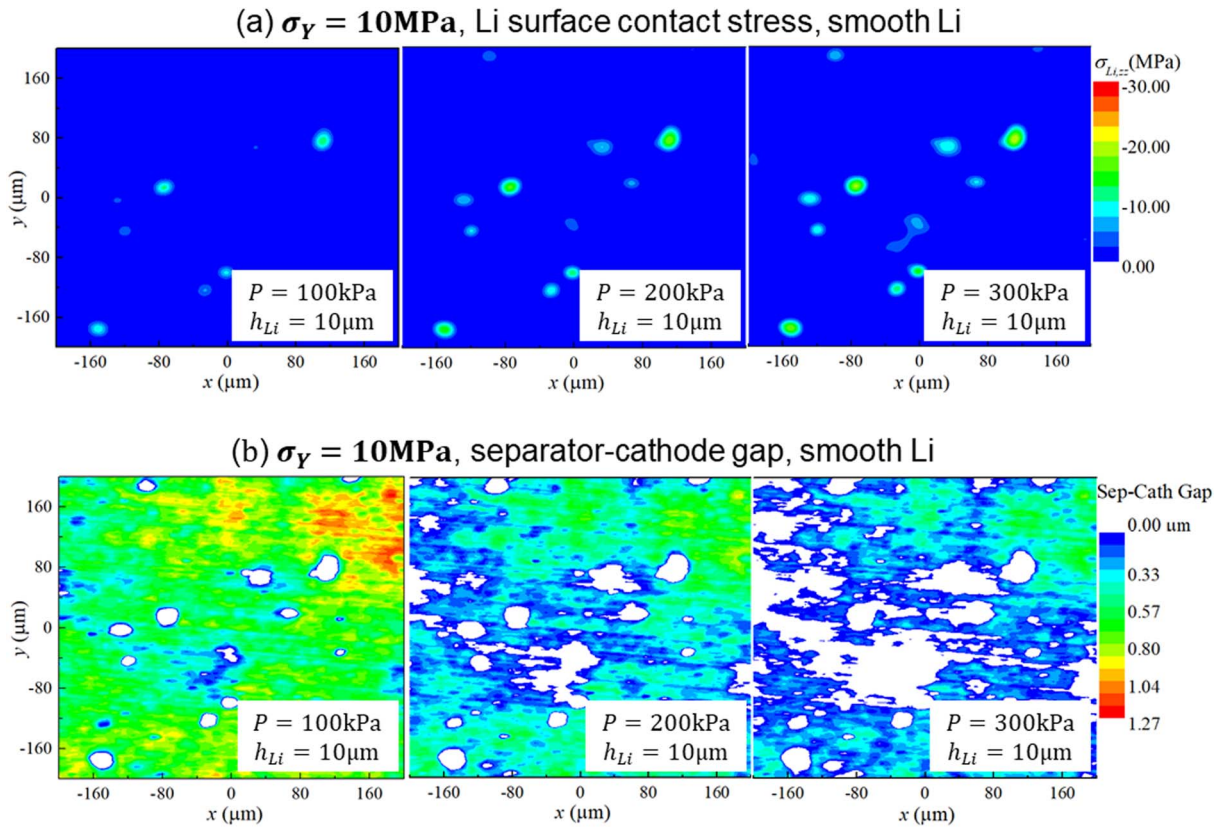

Figure 10. (a) Surface stress contours on Li, and (b) gap contours between the separator and cathode for external pressures of $P = 50$, 200, and 300 kPa, and a Li thickness of $h_{Li} = 10\mu$m, other conditions are same as those in Figure 5. White areas area in contact (gap = 0).

Pressurization of the electrolyte.—A key assumption in the present analysis is that the electrolyte escapes freely from contacting regions of the interface during deformation, and that there is no poroelastic transfer of stress through the liquid. These assumptions should be acceptable, especially at low-moderate contact pressures, given the apparent connectivity in gaps shown in Figure 5. Yet in this figure, there are some islands of contact gap even at low contact pressure, and the degree of percolation deteriorates further at higher pressures. Subsequent creep of the Li or separator could further reduce percolation pathways and increase the possibility of pressurization of trapped electrolyte. Even without fully trapped electrolyte, the Poiseuille equation indicates that electrolyte pressurization may become significant for pore diameters below several tens of nm. Under these circumstances, an internal hydrostatic pressure and smoothing of the stress distribution in the underlying Li may occur. One way to evaluate the contribution of electrolyte pressurization would be to evaluate stress-induced separator pore collapse with and without electrolyte present. Like the experiment described in the previous section, the counterface could be a nondeformable smooth solid such as sapphire, eliminating the complexity of rough Li surfaces. If the electrolyte is trapped, it will suppress pore collapse leading to larger pores in the electrolyte-containing separator compared to the dry separator. Assuming that pore collapse is suppressed to some extent, the degree of pore collapse can be used in conjunction with the properties of the separator to estimate the effective pressure sustained in the electrolyte.

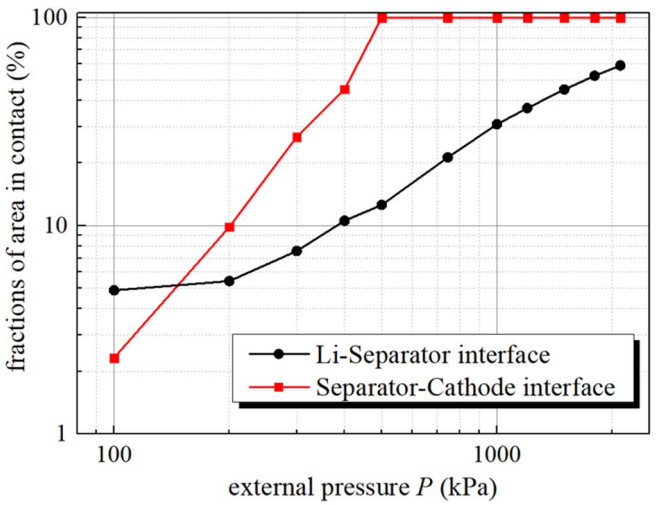

Figure 11. The area in contact as a function of the external pressure. Black line for Li-separator interface, red line for separator-cathode interface.

Li properties.—Li metal has been treated as an elastic-perfectly-plastic material with creep, which is valid[58] for low strain rates ($\leq 3 \times 10^{-4} s^{-1}$) for pure Li. Analyses that include strain-hardening behavior, relevant for high strain rates,[58] may show significant effects during fast charging.

It may be possible to use true, evolving Li surfaces, rather than the idealized Li surfaces analyzed here, once data along these lines[37] is available for cells under pressure.

Conclusions

A 3D electrochemical/contact model has been developed for understanding the effects on plating of Li surface and sub-surface stresses at micro-to-macro scales for electrodes with realistically rough surfaces and under a packing force. This model has a sandwich strucure, containing the Li-separator and separator-cathode interfaces; it considers the Li metal as a rough, elastic-perfectly-plastic material with creep

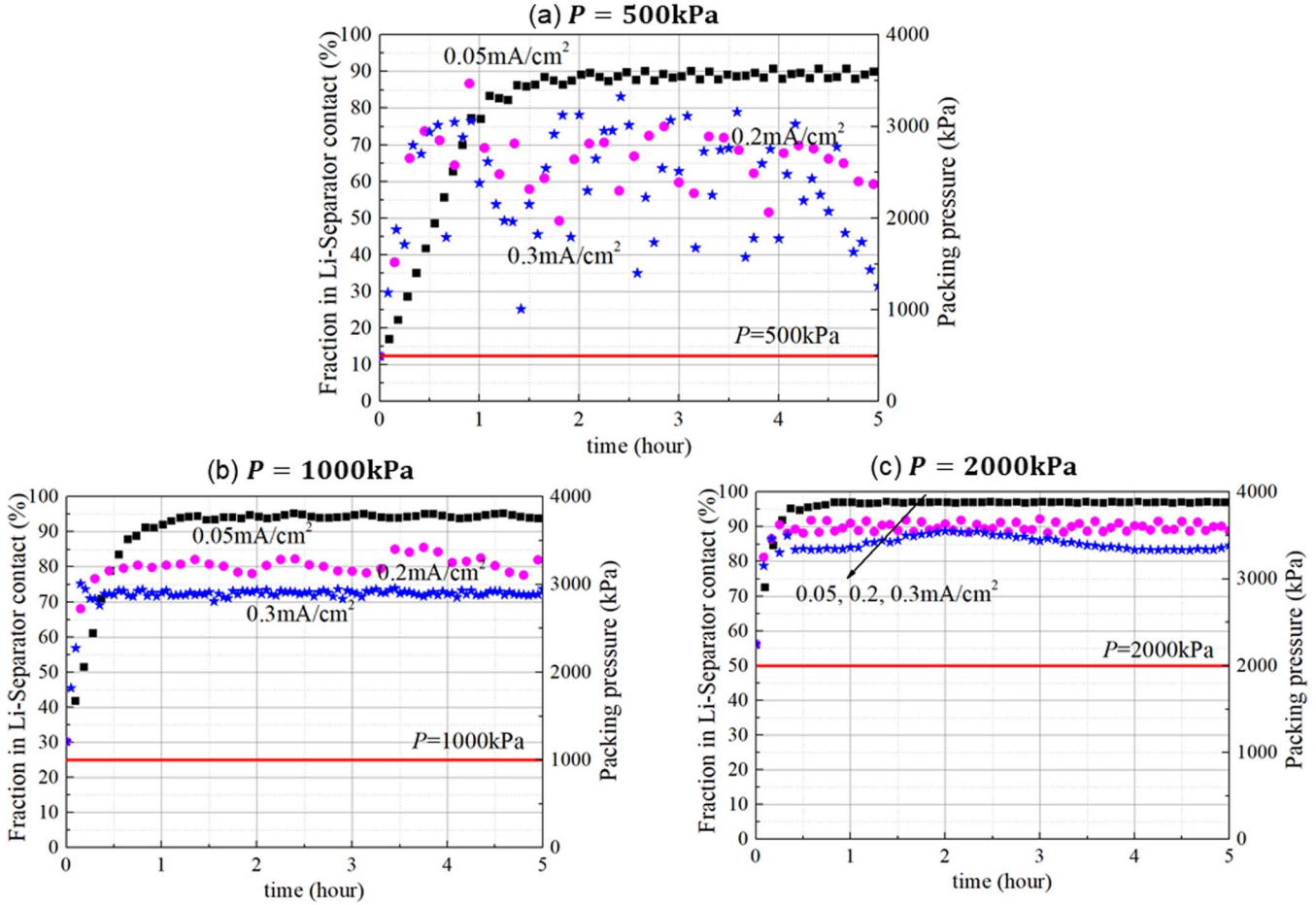

Figure 12. Fraction in Li-separator contact for constant packing pressure $P = 500,\ 1000,\ 2000$kPa.

and the cathode as a rough rigid matererial; it includes the effects of rough surface interactions together with Li plating/stripping.

Our results reveal that contact between the Li metal and the separator is far from conformal, even under high external pressures. Yet, experiment shows[3] that moderate (hundreds of kPa or less) pressures can inhibit growth of Li protrusions, even when the Li protrusion pushes against thin, soft separators. We suggest that flattening of the Li surface can occur with sufficiently high asperity stresses because of an overpotential, creep, and possible pore closure. The higher the current density, the higher the packing pressure needs to be in order create flat Li surfaces in plating/stripping.

We conclude with two thoughts. First, measurements of mechanical properties of Li that has been electroplated in a battery environment are needed. Second, while conformal contact is not necessary to limit dendrite growth, control of cathode roughness may provide a way to inhibit dendrite growth and result in a longer cell life.

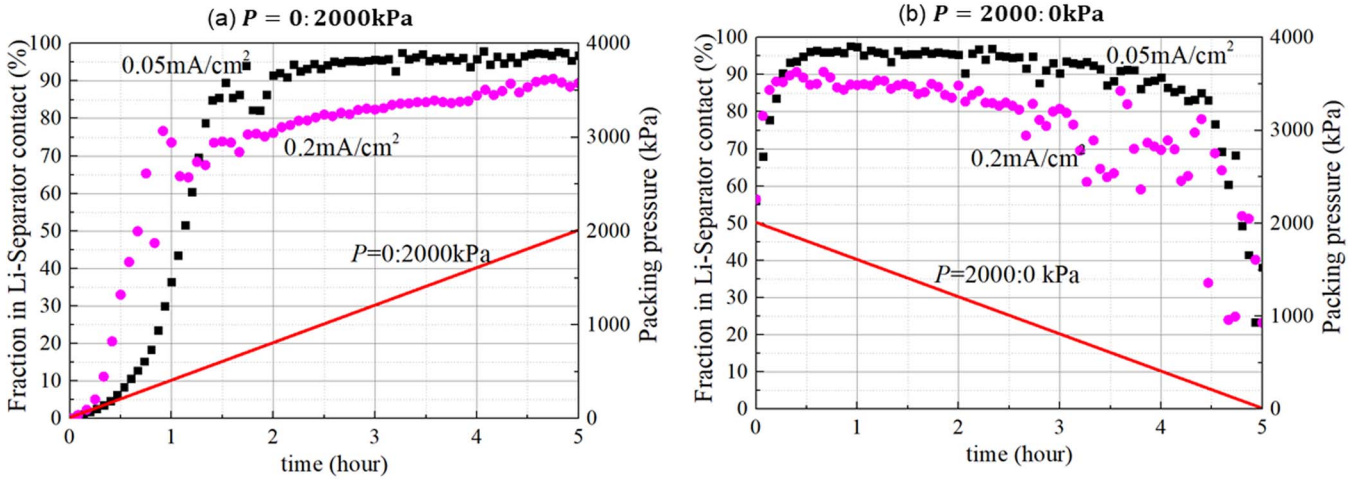

Figure 13. Fraction in Li-separator contact for packing pressure from 0–2000kPa.

Acknowledgments

The authors acknowledge Prof. Y.T. Cheng of University of Kentucky, Prof. Brian Sheldon of Brown University, and Prof. Craig Arnold of Princeton University for valuable discussions. S.J.H. was supported by the Assistant Secretary for Energy Efficiency, Vehicle Technologies Office of the US Department of Energy under the Advanced Battery Materials Research Program. K.L.H, K.L.J., and B.L.B were supported by the Laboratory Directed Research and Development program at Sandia National Laboratories, a multi-mission laboratory managed and operated by National Technology and Engineering Solutions of Sandia, LLC, a wholly owned subsidiary of Honeywell International, Inc., for the U.S. Department of Energy's National Nuclear Security Administration under contract DE-NA0003525.

ORCID

Scott A. Roberts https://orcid.org/0000-0002-4196-6771
Peter M. Attia https://orcid.org/0000-0003-4745-5726
Stephen J. Harris https://orcid.org/0000-0002-5211-3934

References

1. A. Mukhopadhyay and B. W. Sheldon, "Deformation and stress in electrode materials for Li-ion batteries." *Progress in Materials Science*, **63**, 58 (2014).
2. K. N. Wood, M. Noked, and N. P Dasgupta, "Lithium metal anodes: toward an improved understanding of coupled morphological, electrochemical, and mechanical behavior." *ACS Energy Letters*, **2**, 664 (2017).
3. A. J. Louli, M. Genovese, R. Weber, S. Hames, E. Logan, and J. Dahn, "Exploring the Impact of Mechanical Pressure on the Performance of Anode-Free Lithium Metal Cells." *Journal of The Electrochemical Society*, **166**, A1291 (2019).
4. D. Aurbach, E. Zinigrad, Y. Cohen, and H. Teller, "A short review of failure mechanisms of lithium metal and lithiated graphite anodes in liquid electrolyte solutions." *Solid state ionics*, **148**, 405 (2002).
5. L. Gireaud, S. Grugeon, S. Laruelle, B. Yrieix, and J.-M. Tarascon, "Lithium metal stripping/plating mechanisms studies: A metallurgical approach." *Electrochemistry communications*, **8**, 1639 (2006).
6. P. Albertus, S. Babinec, S. Litzelman, and A. Newman, "Status and challenges in enabling the lithium metal electrode for high-energy and low-cost rechargeable batteries." *Nature Energy*, **3**, 16 (2018).
7. Y. Cao, X. Meng, and J. W. Elam, "Atomic Layer Deposition of LixAlyS Solid-State Electrolytes for Stabilizing Lithium-Metal Anodes." *ChemElectroChem*, **3**, 858 (2016).
8. M. Dollé, L. Sannier, B. Beaudoin, M. Trentin, and J.-M. Tarascon, "Live scanning electron microscope observations of dendritic growth in lithium/polymer cells." *Electrochemical and Solid-state Letters*, **5**, A286 (2002).
9. M. Rosso, C. Brissot, A. Teyssot, M. Dollé, L. Sannier, J.-M. Tarascon et al., "Dendrite short-circuit and fuse effect on Li/polymer/Li cells." *Electrochimica Acta*, **51**, 5334 (2006).
10. S. J. Harris and P. Lu, "Effects of Inhomogeneities · Nanoscale to Mesoscale · on the Durability of Li-Ion Batteries." *The Journal of Physical Chemistry C*, **117**, 6481 (2013).
11. P. Bai, J. Li, F. R. Brushett, and M. Z. Bazant, "Transition of lithium growth mechanisms in liquid electrolytes." *Energy & Environmental Science*, **9**, 3221 (2016).
12. S. J. Harris, A. Timmons, and W. J. Pitz, "A combustion chemistry analysis of carbonate solvents used in Li-ion batteries." *Journal of Power Sources*, **193**, 855 (2009).
13. D. Wilkinson, H. Blom, K. Brandt, and D. Wainwright, "Effects of physical constraints on Li cyclability." *Journal of power sources*, **36**, 517 (1991).
14. K. L. Harrison, K. R. Zavadil, N. T. Hahn, X. Meng, J. W. Elam, A. Leenheer et al., "Lithium self-discharge and its prevention: direct visualization through in situ electrochemical scanning transmission electron microscopy." *ACS nano*, **11**, 11194 (2017).
15. T. Hirai, I. Yoshimatsu, and Ji Yamaki, "Influence of electrolyte on lithium cycling efficiency with pressurized electrode stack." *Journal of The Electrochemical Society*, **141**, 611 (1994).
16. L. Liang, Y. Qi, F. Xue, S. Bhattacharya, S. J. Harris, and L.-Q. Chen, "Nonlinear phase-field model for electrode-electrolyte interface evolution." *Physical Review E*, **86**, 051609 (2012).
17. A. Jana, D. R. Ely, and R. E. García, "Dendrite-separator interactions in lithium-based batteries." *Journal of Power Sources*, **275**, 912 (2015).
18. J. Diggle, A. Despic, and J. M. Bockris, "The mechanism of the dendritic electrocrystallization of zinc." *Journal of The Electrochemical Society*, **116**, 1503 (1969).
19. C. Monroe and J. Newman, "Dendrite growth in lithium/polymer systems a propagation model for liquid electrolytes under galvanostatic conditions." *Journal of The Electrochemical Society*, **150**, A1377 (2003).
20. C. Monroe and J. Newman, "The effect of interfacial deformation on electrodeposition kinetics." *Journal of The Electrochemical Society*, **151**, A880 (2004).
21. R. Aogaki and T. Makino, "Theory of powdered metal formation in electrochemistry—Morphological instability in galvanostatic crystal growth under diffusion control." *Electrochimica Acta*, **26**, 1509 (1981).
22. M. Z. Mayers, J. W. Kaminski, and T. F. Miller III, "Suppression of dendrite formation via pulse charging in rechargeable lithium metal batteries." *The Journal of Physical Chemistry C*, **116**, 26214 (2012).
23. R. V. Magan and R. Sureshkumar, "Effect of interfacial reaction rate on the morphogenesis of nanostructured coatings in a simulated electrodeposition process." *Nanotechnology*, **16**, S545 (2005).
24. R. V. Magan, R. Sureshkumar, and B. Lin, "Influence of surface reaction rate on the size dispersion of interfacial nanostructures." *The Journal of Physical Chemistry B*, **107**, 10513 (2003).
25. Z. Li, J. Huang, B. Y. Liaw, V. Metzler, and J. Zhang, "A review of lithium deposition in lithium-ion and lithium metal secondary batteries." *Journal of power sources*, **254**, 168 (2014).
26. C. Brissot, M. Rosso, J.-N. Chazalviel, and S Lascaud, "Dendritic growth mechanisms in lithium/polymer cells." *Journal of power sources*, **81**, 925 (1999).
27. M. Rosso, T. Gobron, C. Brissot, J.-N. Chazalviel, and S. Lascaud, "Onset of dendritic growth in lithium/polymer cells." *Journal of power sources*, **97**, 804 (2001).
28. J.-N. Chazalviel, "Electrochemical aspects of the generation of ramified metallic electrodeposits." *Physical review A*, **42**, 7355 (1990).
29. C. Monroe and J. Newman, "The impact of elastic deformation on deposition kinetics at lithium/polymer interfaces." *Journal of The Electrochemical Society*, **152**, A396 (2005).
30. P. Barai, K. Higa, and V. Srinivasan, "Impact of external pressure and electrolyte transport properties on lithium dendrite growth." *Journal of The Electrochemical Society*, **165**, A2654 (2018).
31. K. Ishiguro, Y. Nakata, M. Matsui, I. Uechi, Y. Takeda, O. Yamamoto et al., "Stability of Nb-Doped Cubic Li7La3Zr2O12 with Lithium Metal." *Journal of The Electrochemical Society*, **160**, A1690 (2013).
32. Y. Ren, Y. Shen, Y. Lin, and C.-W. Nan, "Direct observation of lithium dendrites inside garnet-type lithium-ion solid electrolyte." *Electrochemistry Communications*, **57**, 27 (2015).
33. G. Bucci, B. Talamini, A. Renuka Balakrishna, Y.-M. Chiang, and W. C. Carter, "Mechanical instability of electrode-electrolyte interfaces in solid-state batteries." *Physical Review Materials*, **2** (2018).
34. E. J. Cheng, A. Sharafi, and J. Sakamoto, "Intergranular Li metal propagation through polycrystalline Li6. 25Al0. 25La3Zr2O12 ceramic electrolyte." *Electrochimica Acta*, **223**, 85 (2017).
35. L. Porz, T. Swamy, B. W. Sheldon, D. Rettenwander, T. Frömling, H. L. Thaman et al., "Mechanism of lithium metal penetration through inorganic solid electrolytes." *Advanced Energy Materials*, **7**, 1701003 (2017).
36. L. Cai, K. An, Z. Feng, C. Liang, and S. J. Harris, "In-situ observation of inhomogeneous degradation in large format Li-ion cells by neutron diffraction." *Journal of Power Sources*, **236**, 163 (2013).
37. O. O. Taiwo, D. P. Finegan, J. Paz-Garcia, D. S. Eastwood, A. Bodey, C. Rau et al., "Investigating the evolving microstructure of lithium metal electrodes in 3D using X-ray computed tomography." *Physical Chemistry Chemical Physics*, **19**, 22111 (2017).
38. A. Pei, G. Zheng, F. Shi, Y. Li, and Y. Cui, "Nanoscale nucleation and growth of electrodeposited lithium metal." *Nano Letters*, **17**, 1132 (2017).
39. M. J. Wang, R. Choudhury, and J. Sakamoto, "Characterizing the Li-metal/Solid-electrolyte Interface Dynamics as a function of Stack Pressure and Stripping Current Density." *Joule*. 2019; in press.
40. H. Koshikawa, S. Matsuda, K. Kamiya, M. Miyayama, Y. Kubo, K. Uosaki et al., "Dynamic changes in charge-transfer resistance at Li metal/Li7La3Zr2O12 interfaces during electrochemical Li dissolution/deposition cycles." *Journal of power sources*, **376**, 147 (2018).
41. I. Polonsky and L. M. Keer, "A numerical method for solving rough contact problems based on the multi-level multi-summation and conjugate gradient techniques." *Wear*, **231**, 206 (1999).
42. S. Liu, Q. Wang, and G. Liu, "A versatile method of discrete convolution and FFT (DC-FFT) for contact analyses." *Wear*, **243**, 101 (2000).
43. S. Liu and Q. Wang, "Studying contact stress fields caused by surface tractions with a discrete convolution and fast Fourier transform algorithm." *Journal of tribology*, **124**, 36 (2002).
44. X. Zhang, Z. Wang, H. Shen, and Q. Wang, "An efficient model for the frictional contact between two multiferroic bodies." *International Journal of Solids and Structures*, **130**, 133 (2018).
45. X. Zhang, Z. Wang, H. Shen, and Q. Wang, "Frictional contact involving a multiferroic thin film subjected to surface magnetoelectroelastic effects." *International Journal of Mechanical Sciences*, **131**, 633 (2017).
46. X. Zhang, Z. Wang, H. Shen, and Q. Wang, "Dynamic contact in multiferroic energy conversion." *International Journal of Solids and Structures*, **143**, 84 (2018).
47. Z. Wang, X. Jin, S. Liu, L. M. Keer, J. Cao, and Q. Wang, "A new fast method for solving contact plasticity and its application in analyzing elasto-plastic partial slip." *Mechanics of Materials*, **60**, 18 (2013).
48. Z. Wang, X. Jin, Q. Zhou, X. Ai, L. M. Keer, and Q. Wang, "An efficient numerical method with a parallel computational strategy for solving arbitrarily shaped inclusions in elastoplastic contact problems." *Journal of Tribology*, **135**, 031401 (2013).
49. M. Zhang, Z. Ning, Q. Wang, N. Arakere, Q. Zhou, Z. Wang et al., "Contact elasto-plasticity of inhomogeneous materials and a numerical method for estimating matrix yield strength of composites." *Tribology International*, **127**, 84 (2018).
50. M. Zhang, N. Zhao, P. Glaws, P. Hegedus, Q. Zhou, Z. Wang et al., "Elasto-plastic contact of materials containing double-layered inhomogeneities." *International Journal of Solids and Structures*, **126**, 208 (2017).
51. M. Webster and R. Sayles, "A numerical model for the elastic frictionless contact of real rough surfaces." *Journal of Tribology*, **108**, 314 (1986).
52. Z. Wang, W. Wang, Y. Hu, and H. Wang, "A numerical elastic–plastic contact model for rough surfaces." *Tribology Transactions*, **53**, 224 (2010).

53. X. Zhang, H. Shen, J. Liu, S. Deng, X. Li, Z. Cai et al., "An efficient numerical model for predicting the torsional fretting wear considering real rough surface." *Wear*, **344**, 32 (2015).
54. Q. Zhou, X. Jin, Z. Wang, J. Wang, L. M. Keer, and Q. Wang, "Numerical EIM with 3D FFT for the contact with a smooth or rough surface involving complicated and distributed inhomogeneities." *Tribology International*, **93**, 91 (2016).
55. P. R. Shearing, N. P. Brandon, J. Gelb, R. Bradley, P. J. Withers, A. J. Marquis et al., "Multi Length Scale Microstructural Investigations of a Commercially Available Li-Ion Battery Electrode." *Journal of The Electrochemical Society*, **159**, A1023 (2012).
56. Z. Mao, M. Farkhondeh, M. Pritzker, M. Fowler, and Z. Chen, "Calendar aging and gas generation in commercial graphite/NMC-LMO lithium-ion pouch cell." *Journal of The Electrochemical Society*, **164**, A3469 (2017).
57. E. Logan, E. M. Tonita, K. Gering, J. Li, X. Ma, L. Beaulieu et al., "A study of the physical properties of Li-Ion battery electrolytes containing esters." *Journal of The Electrochemical Society*, **165**, A21 (2018).
58. W. S. LePage, Y. Chen, E. Kazyak, K.-H. Chen, A. J. Sanchez, A. Poli et al., "Lithium Mechanics: Roles of Strain Rate and Temperature and Implications for Lithium Metal Batteries." *Journal of The Electrochemical Society*, **166**, A89 (2019).
59. G. Y. Gor, J. Cannarella, C. Z. Leng, A. Vishnyakov, and C. B. Arnold, "Swelling and softening of lithium-ion battery separators in electrolyte solvents." *Journal of Power Sources*, **294**, 167 (2015).
60. S. Yan, X. Huang, and X. Xiao, "Measurement of the through thickness compression of a battery separator." *Journal of Power Sources*, **382**, 13 (2018).
61. Y. Sheng, C. R. Fell, Y. K. Son, B. M. Metz, J. Jiang, and B. C. Church, "Effect of calendering on electrode wettability in lithium-ion batteries." *Frontiers in Energy Research*, **2**, 56 (2014).
62. C. Meyer, H. Bockholt, W. Haselrieder, and A. Kwade, "Characterization of the calendering process for compaction of electrodes for lithium-ion batteries." *Journal of Materials Processing Technology*, **249**, 172 (2017).
63. C.-W. Wang, Y.-B. Yi, A. Sastry, J. Shim, and K. Striebel, "Particle compression and conductivity in Li-ion anodes with graphite additives." *Journal of The Electrochemical Society*, **151**, A1489 (2004).
64. S. J. Harris, R. D. Deshpande, Y. Qi, I. Dutta, and Y.-T. Cheng, "Mesopores inside electrode particles can change the Li-ion transport mechanism and diffusion-induced stress." *Journal of Materials Research*, **25**, 1433 (2011).
65. Y. Wang and Y.-T. Cheng, "A nanoindentation study of the viscoplastic behavior of pure lithium." *Scripta Materialia*, **130**, 191 (2017).
66. A. Masias, N. Felten, R. Garcia-Mendez, J. Wolfenstine, and J. Sakamoto, "Elastic, plastic, and creep mechanical properties of lithium metal." *Journal of Materials Science*, **54**, 2585 (2019).
67. C. Xu, Z. Ahmad, A. Aryanfar, V. Viswanathan, and J. R. Greer, "Enhanced strength and temperature dependence of mechanical properties of Li at small scales and its implications for Li metal anodes." *Proceedings of the National Academy of Sciences*, **114**, 57 (2017).
68. E. G. Herbert, S. A. Hackney, V. Thole, N. J. Dudney, and P. S. Phani, "Nanoindentation of high-purity vapor deposited lithium films: A mechanistic rationalization of the transition from diffusion to dislocation-mediated flow." *Journal of Materials Research*, **33**, 1361 (2018).
69. A. Masias, N. Felten, R. Garcia-Mendez, J. Wolfenstine, and J. Sakamoto, "Elastic, plastic, and creep mechanical properties of lithium metal." *Journal of Materials Science*, **54**, 2585 (2018).
70. S. Liu, D. Hua, W. W. Chen, and Q. J. Wang, "Tribological modeling: application of fast Fourier transform." *Tribology International*, **40**, 1284 (2007).
71. G. Liu, J. Zhu, L. Yu, and Q. J. Wang, "Elasto-plastic contact of rough surfaces." *Tribology Transactions*, **44**, 437 (2001).
72. X. Yu, Z. Feng, Y. Ren, D. Henn, Z. Wu, K. An et al., "Simultaneous Operando Measurements of the Local Temperature, State of Charge, and Strain inside a Commercial Lithium-Ion Battery Pouch Cell." *Journal of The Electrochemical Society*, **165**, A1578 (2018).
73. R. P. Schultz, *Lithium: Measurement of Young's Modulus and Yield Strength*, Fermi National Accelerator Lab., Batavia, IL (US); 2002.
74. S. Tariq, K. Ammigan, P. Hurh, R. Schultz, P. Liu, and J. Shang, "Li material testing-fermilab antiproton source lithium collection lens." *Proceedings of the 2003 particle accelerator conference:* IEEE; 2003. p. 1452.
75. T. Krauskopf, H. Hartmann, W. G. Zeier, and Janek Jr., "Towards a Fundamental Understanding of the Lithium Metal Anode in Solid State Batteries-An Electrochemo-Mechanical Study on the Garnet-type Solid Electrolyte $Li_{6.25}Al_{0.25}La_3Zr_2O_{12}$." *ACS Applied Materials & Interfaces*, **11**, 14463 (2019).
76. Y. Wang, D. Dang, M. Wang, X. Xiao, and Y. T. Cheng, "Mechanical Properties of Electroplated Mossy Lithium at Room Temperature Measured by Flat Punch Indentation." Submitted for publication.
77. Y. Wang, D. Dang, M. Wang, X. Xiao, and Y. T. Cheng, "Mechanical behavior of electroplated mossy lithium at room temperature studied by flat punch indentation." *Applied Physics Letters*, **115**, 043903 (2019).
78. I. C. Halalay, M. J. Lukitsch, M. P. Balogh, and C. A. Wong, "Nanoindentation testing of separators for lithium-ion batteries." *Journal of Power Sources*, **238**, 469 (2013).
79. X. Su, K. Guo, T. Ma, P. A. Tamirisa, H. Ye, H. Gao et al., "Deformation and chemomechanical degradation at solid electrolyte–electrode interfaces." *ACS Energy Letters*, **2**, 1729 (2017).
80. P. Barai, K. Higa, and V. Srinivasan, "Effect of initial state of lithium on the propensity for dendrite formation: a theoretical study." *Journal of The Electrochemical Society*, **164**, A180 (2017).
81. L. H. He and M. V. Swain, "Nanoindentation creep behavior of human enamel." *Journal of Biomedical Materials Research Part A: An Official Journal of The Society for Biomaterials, The Japanese Society for Biomaterials, and The Australian Society for Biomaterials and the Korean Society for Biomaterials*, **91**, 352 (2009).
82. A. Bower, N. A. Fleck, A. Needleman, and N. Ogbonna, "Indentation of a power law creeping solid." *Proceedings of the Royal Society of London Series A: Mathematical and Physical Sciences*, **441**, 97 (1993).
83. J. Alkorta, J. M. Martínez-Esnaola, and J. G. Sevillano, "On the elastic effects in power-law indentation creep with sharp conical indenters." *Journal of Materials Research*, **23**, 182 (2008).
84. J. Michael and R. C. Wang, "Jeff Sakamoto. Characterizing the Li-metal/Solid-electrolyte Interface Dynamics as a function of Stack Pressure and Stripping Current Density." *Joule*. 2019:Accepted.
85. W. Li, H. Yao, K. Yan, G. Zheng, Z. Liang, Y.-M. Chiang et al., "The synergetic effect of lithium polysulfide and lithium nitrate to prevent lithium dendrite growth." *Nature Communications*, **6**, 7436 (2015).
86. P. Lu, C. Li, E. W. Schneider, and S. J. Harris, "Chemistry, Impedance, and Morphology Evolution in Solid Electrolyte Interphase Films during Formation in Lithium Ion Batteries." *The Journal of Physical Chemistry C*, **118**, 896 (2014).
87. P. Lu and S. J. Harris, "Lithium transport within the solid electrolyte interphase." *Electrochemistry Communications*, **13**, 1035 (2011).
88. X. Fan, L. Chen, O. Borodin, X. Ji, J. Chen, S. Hou et al., "Non-flammable electrolyte enables Li-metal batteries with aggressive cathode chemistries." *Nature Nanotechnology*, **13**, 715 (2018).
89. X. Ren, Y. Zhang, M. H. Engelhard, Q. Li, J.-G. Zhang, and W. Xu, "Guided lithium metal deposition and improved lithium coulombic efficiency through synergistic effects of LiAsF6 and cyclic carbonate additives." *ACS Energy Letters*, **3**, 14 (2017).
90. J. Wang, W. Huang, A. Pei, Y. Li, F. Shi, X. Yu et al., "Improving cyclability of Li metal batteries at elevated temperatures and its origin revealed by cryo-electron microscopy." *Nature Energy*, **4**, 664 (2019).
91. L. Li, S. Basu, Y. Wang, Z. Chen, P. Hundekar, B. Wang et al., "Self-heating–induced healing of lithium dendrites." *Science*, **359**, 1513 (2018).
92. C. Peabody and C. B. Arnold, "The role of mechanically induced separator creep in lithium-ion battery capacity fade." *Journal of Power Sources*, **196**, 8147 (2011).
93. J. Cannarella and C. B. Arnold, "Ion transport restriction in mechanically strained separator membranes." *Journal of Power Sources*, **226**, 149 (2013).
94. J. Cannarella and C. B. Arnold, "Stress evolution and capacity fade in constrained lithium-ion pouch cells." *Journal of Power Sources*, **245**, 745 (2014).
95. J. Cannarella and C. B. Arnold, "The effects of defects on localized plating in lithium-ion batteries." *Journal of The Electrochemical Society*, **162**, A1365 (2015).
96. X. M. Liu, A. Fang, M. P. Haataja, and C. B Arnold, "Size dependence of transport non-uniformities on localized plating in lithium-ion batteries." *Journal of The Electrochemical Society*, **165**, A1147 (2018).